Epsins oversee smooth muscle cell reprograming by influencing master regulators KLF4 and OCT4

Beibei Wang[1]*, Kui Cui[1]*, Bo Zhu[1]*, Yunzhou Dong[1], Donghai Wang[1], Bandana Singh[1], Hao Wu[1], Kathryn Li[1], Shahram Eisa-Beygi[1], Yong Sun[2], Scott Wong[1], Douglas B. Cowan[1], Yabing Chen[2], Mulong Du[3]△, Hong Chen[1]△

[1] Vascular Biology Program, Boston Children's Hospital and Department of Surgery, Harvard Medical School, Boston, MA, 02115, USA

[2]Department of Pathology, Birmingham, AL 35294, USA; University of Alabama at Birmingham, and the Birmingham Veterans Affairs Medical Center, Birmingham, AL 35294, USA

[3]Department of Environmental Health, Harvard T.H. Chan School of Public Health, 655 Huntington Avenue, Boston, MA, 02115, USA

△Correspondence to: Hong Chen, PhD, Email hong.chen@childrens.harvard.edu or Mulong Du, PhD, [2]Department of Environmental Health, Harvard T.H. Chan School of Public Health, 655 Huntington Avenue, Boston, MA, 02115, Email mulongdu@hsph.harvard.edu

* B. Wang, K. Cui, and B. Zhu, contributed equally.

Abstract

Smooth muscle cells in major arteries play a crucial role in regulating coronary artery disease. Conversion of smooth muscle cells into other adverse cell types in the artery propels the pathogenesis of the disease. Curtailing artery plaque buildup by modulating smooth muscle cell reprograming presents us a new opportunity to thwart coronary artery disease. Here, our report how Epsins, a family of endocytic adaptor proteins oversee the smooth muscle cell reprograming by influencing master regulators OCT4 and KLF4. Using single-cell RNA sequencing, we characterized the phenotype of modulated smooth muscle cells in mouse atherosclerotic plaque and found that smooth muscle cells lacking epsins undergo profound reprogramming into not only beneficial myofibroblasts but also endothelial cells for injury repair of diseased endothelium. Our work lays concrete groundwork to explore an uncharted territory as we show that depleting Epsins bolsters smooth muscle cells reprograming to endothelial cells by augmenting OCT4 activity but restrain them from reprograming to harmful foam cells by destabilizing KLF4, a master regulator of adverse reprograming of smooth muscle cells. Moreover, the expression of Epsins in smooth muscle cells positively correlates with the severity of both human and mouse coronary artery disease. Integrating our scRNA-seq data with human Genome-Wide Association Studies (GWAS) identifies pivotal roles Epsins play in smooth muscle cells in the pathological process leading to coronary artery disease. Our findings reveal a previously unexplored direction for smooth muscle cell phenotypic modulation in the development and progression of coronary artery disease and unveil Epsins and their downstream new targets as promising novel therapeutic targets for mitigating metabolic disorders.

Introduction

Atherosclerosis is a chronic inflammatory disease characterized by the progressive formation of plaques on the arterial walls that constitutes the primary pathological process for the development and progression of coronary artery disease (CAD)[1,2]. In advanced stage of the disease, rupture of the atherosclerotic plaques causes atherosclerotic thrombosis[3] leading to life-threatening consequences such as myocardial infarction and stroke[4]. Aortic smooth muscle cells (SMCs) are one of the major cellular components of the atherosclerotic plaques[5], contributing to the formation of both the fibrous cap and the necrotic core via a process called SMC phenotypic modulation or switching[6]. A paradigm largely built on results from *in vitro* studies seemed to suggest that during atherosclerosis, SMCs migrate into intimal space, proliferate, and transdifferentiate into macrophage-like phenotypes characterized by the expression of *Lgals3* and acquired increased phagocytic activity[7-9]. Those proinflammatory macrophage-adopting SMCs engulf oxidized lipid and dead cells[10] and eventually become foam cells that enlarge lipid-laden necrotic core and destabilizes plaques[11]. Whereas other studies highlight the conversion of SMCs into synthetic SMC phenotypes which could contribute to the protective fibrous plaque cap and stabilizing plaques[6,8,11]. Utilizing genetic lineage tracing and single cell RNA sequencing techniques, one recent study elucidated that in atherosclerotic lesions SMCs transdifferentiate into a fibroblast-like phenotypes (referred to as myofibroblasts) that express Lgals3 with acquired lipid-phagocytosis capacity. Very few, if any, SMC-derived macrophage like cells were identified in this study[12]. Those myofibroblasts

strengthen the fibrous cap and therefore stabilize the plaques[12]. Whereas using a similar approach, another study identified the emergence of a population of stem, endothelial and monocyte/macrophage (SEM) lineage cells derived from SMC in response to atherosclerotic stimuli in addition to significant number of SMC-derived macrophage like cells in the atherosclerotic lesions[13]. Those SMC-derived SEM cells have the potential to differentiate further into macrophages, fibrochondrocytes as well as SMCs[13]. While the SEM lineage of cells express the endothelial marker Vcam-1, the potency of those cells to differentiate into endothelial cells (ECs) to participate in endothelial repair in atherosclerotic lesions has not been investigated.

Krüppel-like factor 4 (KLF4) is a zinc finger transcription factor that plays a critical role in cell fate decision[14]. Numerous studies have shown the arthero-prone function of KLF4 in SMCs[7,15]. KLF4 controls SMC phenotypic plasticity by suppressing the expressions of SMC markers *Acta2*, *Tagln*, *Myh11*, and *Cnn1*[7,16]. Interestingly, the stability of KLF4 is regulated by posttranslational modifications such as methylation and ubiquitination. VHL3-mediated ubiquitination promotes KLF4 degradation by proteosomes whereas methylation inhibits KLF4 ubiquitination, therefore enhances KLF4 protein level[17]. In sharp contrast to KLF4, the stem cell pluripotent transcription factor OCT4 in SMCs is athero-protective in that SMC-specific deletion of OCT4 led to increased size of necrotic core and decreased fibrous plaque cap, and therefore destabilized plaques[18]. A recent study further demonstrated that OCT4 is activated and inhibits intima formation after vascular injury[19]. Those phenotypes in OCT4-SMC knockout mice are exactly the opposite to KLF4-SMC knockout mice[7]. Further studies employing chromatin immunoprecipitation and sequencing (chipseq) identified that KLF4 and OCT4 control nearly opposite patterns of gene expression in SMC[15]. How the counteracting function of KLF4 and OCT4 is coordinated during SMC phenotypic switching remains unclear.

The Epsin family of endocytic adaptors including Epsin1 and Epsin2 plays an essential role in the pathology of atherosclerosis via regulating endothelial-to-mesenchymal transition of ECs, as well as lipid uptake, cholesterol efflux, and IP3R1 degradation in macrophages within the atherosclerotic lesions[20-22]. Nevertheless, whether SMC-intrinsic Epsins contribute to the regulation of SMC plasticity, and atherosclerotic pathogenesis has not been explored. Recent studies suggest that Epsins are crucial for transforming growth factor (TGF)-beta receptor endocytosis and signaling[20] in ECs. TGF-beta activates the *Acta2* (encoding αSMA) expression through promoting KLF4 degradation[23,24]. However, whether Epsins control SMC phenotypic switching through regulating KLF4 stability has not been investigated.

In this study, we profiled cellular components of aortae isolated from atherosclerotic mice at the single-cell level and explored the role of SMC-intrinsic Epsins in the pathogenesis of atherosclerosis. We identified a unique cluster of endothelial-like cells transdifferentiated from SMCs in the atherosclerotic aortae. Those endothelial-like cells can integrate into intima and participate in the repair of endothelial injury caused by atherosclerotic stimuli. *In vitro*, those ECs are equipped with acetylated-low density lipoprotein (ac-LDL) endocytosis capacity. Loss of expression of Epsins in SMCs, on one hand, enhanced KLF4 degradation and therefore promoted SMC marker gene expression. On the other hand, Epsins-deficiency promotes trans-differentiation of SMCs into endothelial-like cells by increasing the protein level of OCT4. At the molecular level, Epsins stabilize KLF4 through inhibiting ubiquitinated KLF4 degradation by directly binding to KLF4 through the Epsins' ENTH+UIM domain. Mice deficient for both

Epsins1&2 specifically in SMCs are more resistant to western diet-induced atherosclerosis. Those findings uncovered a novel function that is independent of Epsins' endocytic activity in promoting the pathogenesis of atherosclerosis.

STAR METHODS

Mice

All animal experiments followed institutional guidelines. Mouse protocols were approved by the Institutional Animal Care and Use Committee (IACUC) of Boston Children's Hospital, MA, United States.

All mice including *ApoE*$^{-/-}$ mice (stock#002052, Jackson Research Laboratory) and *Epsin1*$^{fl/fl}$*;Epsin2*$^{-/-}$ mice used are backcrossed to C57BL/6 (stock#00664, Jackson Research Laboratory) genetic background. SMC-specific deletion of Epsin was established by crossing *Epsin1*$^{fl/fl}$*;Epsin2*$^{-/-}$ mice with SMC-specific SMMHC (*Myh11*)-*iCreER*^{T2} transgenic mice (stock# 019079, Jackson Research Laboratory)[25] as *Epsin1*$^{fl/fl}$*;Epsin2*$^{-/-}$*/Myh11-iCreER*^{T2} mice. *Epsin1*$^{fl/fl}$*;Epsin2*$^{-/-}$*/Myh11-iCreER*^{T2} mice were further crossed to *ApoE*$^{-/-}$ background to generate the compound mutant mouse strain-*Epsin1*$^{fl/fl}$*;Epsin2*$^{-/-}$*/Myh11-iCreER*^{T2}*/ApoE*$^{-/-}$. The details of the SMC-specific deletion of Epsin and *ApoE*$^{-/-}$ control mice used in this study were described in Figure S1E. *Myh11-iCreER*^{T2}-eYFP$^{stop/fl}$ mice were bred to *ApoE*$^{-/-}$ mice to generate *Myh11-iCreER*^{T2}-eYFP$^{stop/fl}$*/ApoE*$^{-/-}$ mice as controls. These mice were further bred to *Epsin1*$^{fl/fl}$*;Epsin2*$^{-/-}$*/Myh11-iCreER*^{T2}*/ApoE*$^{-/-}$ mice to establish *Epsin1*$^{fl/fl}$*;Epsin2*$^{-/-}$*/Myh11-iCreER*^{T2}-eYFP$^{stop/fl}$*/ApoE*$^{-/-}$ mice. The details of the SMC-lineage tracing mice and control mice were described in Figure S5B. *Myh11-iCreER*^{T2} bacterial artificial chromosome transgene is localized on the Y chromosome, so only male mice were used[26]. 10 μg/g body weight of 4-Hydroxytamoxifen were injected intraperitoneally to induce SMC-specific deletion of *Epsins* and to activate the *eYFP* gene expression at 6 to 8 weeks of age. Then, the mice were fed a western diet (D12079B, New Brunswick, USA) for 9-20 weeks.

Primary Mouse SMCs Isolation

Mice were anesthetized with isoflurane. Thoracic aortas were harvested from mice and placed in 1× Hank's balanced salt solution (HBSS) supplemented with penicillin and streptomycin (P/S) at 4°C for 1 hr. Vessels were placed in a sterile culture plate and enzyme solution (Collagenase Type I 5 mg/mL + Collagenase Type IV 5 mg/mL + Liberase Blendzyme 3 0.4 U/mL) was added to cover the vessels. The plates were placed in a 37°C incubator for 2 mins. The aortas were transferred to DMEM medium and cut open longitudinally with scissors. The adventitial layer and EC layer were removed, the muscularis layer was incubated at 37°C for approximately 15 mins. Next, the muscularis layer of aortae were dissected into smaller pieces. The aortic pieces were then carefully removed and placed into 4% gelatin coated 6-well plate, covered with sterile 22 × 22 mm cover slip and supplemented with 1 mL complete DMEM medium containing 20% FBS, 1% insulin-transferrin-selenium, 10 ng/mL epidermal growth factor and 1% P/S. Plates were placed in a 37°C, 5% CO_2 culture incubator and the cell medium was refreshed every 3-4 days. As cells expanded and started to cover area (approximately 7 days), the cover slips were flipped, and cells were seeded into a new 6-well plate (cell side up) and covered with 2 mL complete DMEM medium. The residual tissue pieces were removed from the plate and cells were refed in original plate. Cells were allowed to

153 continue to grow until they reach confluence. Cells were weaned into 10% FBS complete
154 DMEM media after 3-5 passages, depending on their viability.
155
156 **Small interfering RNA (siRNA) Transfection**
157 siRNA transfection was performed according to the manufacturer's instructions. Briefly,
158 primary SMCs were transfected by RNAiMAX (CAT#13778, Invitrogen) with either
159 scrambled siRNA duplex or Epsin1 (UGCUCUUCUCGGCUCAAACUAAGGG) or Epsin2
160 siRNA duplexes (AAAUCCAACAGCGUAGUCUGCUGUG) designed by Ambion®
161 Silencer® Select Predesigned siRNAs (Invitrogen), or ON-TARGETplus Mouse Pou5f1
162 siRNA (CAT#J-046256-05-002, Invitrogen). At 48 hrs post transfection, cells were processed
163 for western blot assays.
164
165 **Immunofluorescent Staining**
166 Human samples: All human samples are from Maine Health Institute for Research Biobank,
167 Maine Medical Center, the details of the samples were described previously[22]. Samples were
168 deparaffinized twice in xylene (15 mins for each time), immersed in graded ethanol (100%,
169 100%, 95%, 90%, 80%, and 70%, each for 3 mins), washed in running tap water. After blocking
170 endogenous peroxidase activity, the samples were blocked in blocking buffer (PBS with 3%
171 donkey serum, 3% BSA and 0.3% Triton X-100), and incubated with the primary antibodies,
172 anti-αSMA and Epsin1, Epsin2, KLF4 or VHL (1:70 to 1:300 dilution in blocking buffer), 4°C
173 overnight. Respective secondary antibodies conjugated to fluorescent labels (Alexa Flour 488
174 or 594; 1:200) were added for 2 hrs at room temperature. The sections were mounted with
175 Fluoroshield™ histology mounting medium with DAPI.
176 Mouse samples: Mouse aortic root and brachiocephalic trunk cryosections were heated to
177 room temperature for 30 mins, fixed in 4% paraformaldehyde for 15 mins and blocked in
178 blocking buffer for 1 hr. Sections were then incubated with the primary antibodies4°C
179 overnight, followed by incubation with the respective secondary antibodies conjugated to
180 fluorescent for 2 hrs at room temperature. The sections were mounted with Fluoroshield™
181 histology mounting medium containing DAPI.
182 Cell staining: SMCs were plated on the 18 mm coverslips and washed with PBS for 3 times,
183 fixed in 4% paraformaldehyde for 15 mins and blocked with blocking buffer for 1 hr.
184 Coverslips were incubated with the primary antibodies, 4°C overnight, followed by incubation
185 with the respective secondary antibodies conjugated to fluorescent labels for 1 hr at room
186 temperature. Antibody list, clones and catalogue numbers used for staining are provided in the
187 Table S1. The sections were mounted with Fluoroshield™ histology mounting medium
188 containing DAPI. Immunofluorescent images were captured using a Zeiss LSM880 confocal
189 microscope and analyzed with ZEN-Lite 2012 software and HIH ImageJ software.
190
191 **Atherosclerotic Lesion Characterization**
192 The whole aortae were collected and fixed in 4% paraformaldehyde. Next, the aortas were
193 stained with Oil Red O for *en face* analysis. Hearts and brachiocephalic trunk were embedded
194 in O.C.T and sectioned at 8 microns. Lesion area of the aortic root was quantified by
195 hematoxylin and eosin staining. Neutral lipids deposition was determined by Oil Red O
196 staining. Aortic lesion size and lipid content of each animal were obtained by an average of

three sections from the same mouse.

En face Oil Red O Staining

Whole aortae were dissected symmetrically, pinned to parafilm to allow the *en face* exposed and fixed in formalin for 12 hrs. The aortae were washed in PBS for 3 times and rinsed in 100% propylene glycol, followed by staining with 0.5% Oil Red O solution for 20 mins at 65°C. The samples were then put in 85% propylene glycol for 2 mins, followed by three washes in DD Water. Slides were next incubated with hematoxylin for 30 sec, rinsed in running tap water. Imaging was performed using a Nikon SMZ1500 stereomicroscope, SPOT Insight 2Mp Firewire digital camera, and SPOT Software 5.1.

Oil Red O Staining of Cryostat Section

Cryostat sections of mouse aortic root and brachiocephalic trunk were washed in PBS for 2 mins, then fixed in 4% paraformaldehyde for 5 mins. Slices were washed in PBS followed by staining with freshly prepared 0.5% Oil Red O solution in isopropanol for 10 mins at 37°C. Slices were then put in 60% isopropanol for 30 sec, followed by 3 washes in water. Slices were next incubated with hematoxylin for 30 sec, rinsed in running tap water, and mounted with 90% Glycerin.

Hematoxylin and Eosin Staining

Cryostat sections of mouse aortic root and brachiocephalic trunk were washed in PBS for 2 mins, then fixed in 4% paraformaldehyde for 5 mins. Next, slides were stained with 0.1% hematoxylin for 2 mins followed by washing under running tap water for 2 mins. Slices were then dipped in Eosin working solution for 20 sec, quickly rinsed with tap water, dehydrated using graded ethanol (95% and 100% ethanol), followed by rendering of samples transparent by incubation in 100% xylene for 1 min. Slices were mounted in synthetic resin.

Van Gieson's Staining

Van Gieson's staining was performed based on manufacturer's instructions. In brief, Cryostat sections of mouse aortic root and brachiocephalic trunk were washed in PBS for 2 mins, then fixed in 4% paraformaldehyde for 5 mins. Slices were placed in Elastic Stain Solution (5% hematoxylin + 10% ferric chloride + Lugol's lodine Solution) for 20 mins, then rinsed under running tap water. Then, slices were dipped in differentiating solution 20 times and in sodium thiosulfate solution for 1 min, following with rinsing under running tap water. Slices were dehydrated in 95% and 100% alcohol once, respectively, cleared and mounted in synthetic resin.

RNA Isolation and Quantitative Real-time PCR

Total RNA was extracted using RNeasy® Mini Kit, based on manufacturer's instruction. cDNA was synthetized by reverse transcription using the iScript cDNA Synthesis Kit (Bio-Rad Laboratories, CA, United States). Quantitative PCR (qPCR) was performed with specific primers using SYBR® Green PCR Master Mix reagent in StepOnePlus Real-Time PCR System. Cdna-specific primers can be found in Table S2.

241 **Immunoprecipitation and Western Blotting**

242 For immunoprecipitation, SMCs were lysed with RIPA buffer (50 mM Tris, pH 7.4, with
243 150 mM NaCl, 1% Nonidet P-40, 0.1% SDS, 0.5% sodium deoxycholic acid, 0.1% sodium
244 dodecyl sulfate, 5 mM N-ethylmaleimide and protease inhibitor cocktail). For KLF4
245 ubiquitination experiments, SMCs were lysed using denaturing buffer (1% SDS in 50 mM Tris,
246 pH 7.4) and boiled at 95°C for 10 mins to denature protein complexes. Lysates were re-natured
247 using nine volumes of ice-cold RIPA buffer, then prepared for immunoprecipitation as follows:
248 Cell lysates were pre-treated with Protein A/G PLUS-Agarose (sc-2003, Santa Cruz
249 Biotechnology) at 4°C for 2 hrs to remove nonspecific protein, followed by centrifugation at
250 12000 rpm for 5 mins at 4°C. Supernatant was transferred to a new tube, incubated with Protein
251 A/G PLUS-Agarose and antibodies against Epsin1 or KLF4 or ubiquitin at 4°C overnight.
252 Mouse IgG was used as negative control. Protein A/G beads were washed with RIPA buffer for
253 2 times, followed by PBS for 1 time. Then, beads were suspended with 80 μL 2× loading buffer
254 and heated at 95°C for 10 mins. After centrifugation, precipitated proteins were visualized by
255 Western blot. Proteins were resolved by SDS-PAGE gel and electroblotted to nitrocellulose
256 membranes. NC membranes were blocked with 5% milk (w/v) and blotted with antibodies.
257 Western blots were quantified using NIH Image J software.

258

259 **Differentiation of SMCs to EC Phenotype**

260 EC function was tested with DiI-ac-LDL Staining Kit based on manufacturer's instructions.
261 Briefly, SMCs were planted onto 12-mm slides until they reached 95% confluence. Next, the
262 cells were treated with 100 μg/mL oxLDL for 4 days. Then, 10 μg/mL DiI-ac-LDL (CAT#022K,
263 Cell Applications) was added, instead of oxLDL, in the medium onto each 12-mm slide. The
264 slides were placed in a 37°C, 5% CO_2 incubator for 6 hrs. The cells were washed 3 times with
265 a wash buffer. The slides were mounted with a cover slip using mounting solution. Images were
266 taken using a Zeiss LSM880 confocal microscope and analyzed with HIH ImageJ software.

267

268 **Flow Cytometry and Cell Sorting**

269 Prepare a single cell suspension isolated from eYFP-SMC mice aorta, thoracic aortae were
270 isolated as previously reported. The aortae were cut into small pieces and moved into a new
271 dish containing enzyme solution, incubated at 37°C in the incubator for about 1 hr. After an
272 hour, the plates were washed with 2 mL warmed DMEM medium (DMEM + 5% FBS + P/S).
273 Cells were collected by spinning 1500 rpm for 5 mins. The supernatant was carefully removed
274 and 0.5 mL sterile PBS containing 1% BSA was added. Total eYFP-tagged SMCs were sorted
275 as live by using BD FACSARIA II.

276 Single-cell suspensions used for intracellular staining were fixed in ice-cold 4% PFA,
277 following treatment with 150 μL permeabilization buffer (1% Triton X-100 in PBS). Next, 1
278 μg blocking IgG was added and the samples were incubated at room temperature for 15 mins.
279 Intracellular cytokines were stained with antibodies against CD31, VE-Cadherin, KLF4 or
280 OCT4. Total eYFP-tagged SMCs were sorted as live, $CD31^+$ or VE-$Cadherin^+$ for KLF4 or
281 OCT4 expression in *Epn1&2-SMC*^{iDKO}*/eYFP*$^{+/-}$*/ApoE*$^{-/-}$ and *eYFP*$^{+/-}$*/ApoE*$^{-/-}$ mice. Antibody
282 list, clones and catalogue numbers used for staining were provided in Table S1. BD FACSARIA
283 II was used to collect raw data from flow cytometry experiments. All data files were analyzed
284 using FlowJo version 9.

Cell Culture and Plasmids Transfection

The HEK 293T cell line (ATCC no. CRL-11268) was used for plasmid transfection to map the binding sites of Epsin to KLF4. Flag-tagged Epsin1WT, Epsin1ΔUIM, Epsin1ΔENTH truncation constructs, and pcDNA vector were prepared previously in our lab. pCX4-KLF4 (Plasmid #36118) were purchased from AddGene. HEK 293T cells were cultured in DMEM (10% FBS and 1% Pen-Strep) at 37°C in humidified air containing 5% CO_2 atmosphere and transfected using Lipofectamine 2000 as instructed by the manufacturer.

The primary SMCs isolated from *Epn1&2-SMC^{iDKO}/eYFP$^{+/-}$/ApoE$^{-/-}$* were infected with adenovirus (Ad)-KLF4 or Ad-null for 48 hrs[27]. Ad-KLF4 and Ad-null are gifts from Dr. John Y.-J. Shyy, University of California, San Diego.

Single-cell Preparation and Data Processing

Single cell of mouse arterial specimens was prepared as above. The cell viability exceeded 90% and was determined under the microscope with trypan blue staining. 20 μL of cell suspension was calculated to contain ~20,000 cells for each sample. Single-cell capturing and library construction were performed using the Chromium Next GEM Single Cell 3' Reagent Kits v3.1 (10× Genomics) according to the manufacturer's instructions. In brief, 50 μL of barcoded gel beads, 45 μL partitioning oil and 70 μL cell suspension were loaded onto the Chromium Next GEM Chip G to generate single-cell gel beads-in-emulsion. Captured cells were lysed and the transcripts were reverse-transcribed inside individual gel beads-in-emulsion. Full-length cDNA along with cell barcodes were amplified via PCR. The sequencing libraries were constructed by using the 3' Library Kits. Each sample was processed independently. The constructed libraries were sequenced on an Illumina NovaSeq platform.

Similar to the method employed in our previous study[20], raw sequencing data of FASTQ files were processed using CellRanger (version 3.0.2, 10× Genomics) with default parameters and mapped to mouse reference genome mm10, as well as annotated via a Ensembl 93 annotation, to generate matrices of gene counts by cell barcodes. We used *Seurat* package[28] to conduct quality controls and downstream analyses. For quality controls, genes expressed in less than 10 cells and cells with less than 100 genes were initially removed from the datasets. The subsequent filters at the cell level met the following criteria of number of genes detected per cell > 250, number of UMIs per cell > 500, log10 transformed number of genes detected per UMI > 0.8, and mitochondrial counts ratio < 0.2. Raw unique molecular identifier (UMI) counts were normalized and regressed by mitochondrial mapping percentage using *SCTransform* function. Possible batch effects derived from different conditions on mouse models were adjusted using *Harmony* package[29]. Dimension reduction was performed using principal-component analysis (PCA) with *RunPCA* function. Two-dimensional Uniform Manifold Approximation and Projection (UMAP) was used for visualization. Graph-based clustering was performed on the integrated dataset with a default method of K-nearest neighbor (KNN) graph. Cell clusters were identified using the graph observed above with a resolution parameter ranging from 0.1 to 1.2. In this study, we divided cells into 26 clusters underlying the resolution parameter of 0.8, which were further grouped into 10 cell subgroups.

Cleavage Under Targets and Tagmentation (CUT&Tag)

329 SMCs isolated from aortae of both *ApoE*$^{-/-}$ and *Epn1&2-SMC*^{iDKO}*/ApoE*$^{-/-}$ mice (n=3) were
330 subjected for CUT&Tag assay protocol according Henikoff's lab with minor modification[30].
331 Briefly, 100,000 isolated VSMCs were bund to Concanavalin-A-coated beads, and then bind
332 primary antibodies of KLF4 and OCT4 (1:100 dilution) to the cell and Concanavalin A-coated
333 beads complex for overnight at 4 °C. The pig-anti-rabbit secondary antibody (1:100 dilution)
334 was added into the mixture above for 1 hr incubation. After secondary antibody incubation, the
335 mixture was washed by Dig-wash buffer twice, bind pAG-Tn5 adapter complex for 1 hr, and
336 then washed by Dig-300 buffer twice. The complex mixture was incubated at 37°C for
337 tagmentation for 1 hr. After tagmentation, DNA fragments were extracted and further for PCR
338 and post-PCR clean-up. Finally, the established libraries were sent for DNA sequencing.
339 We followed the pipeline https://yezhengstat.github.io/CUTTag_tutorial to analyze the
340 CUT&Tag data. Briefly, sequence reads that passed the quality control by FastQC were aligned
341 to the mm10 mouse reference genome using Bowtie2. Peak calling was performed by *SEACR*
342 R package (PMID: 31300027), which provided enriched regions from chromatin profiling data.
343 *DESeq2* R package (PMID: 25516281) was used to analyze the differential enriched peaks of
344 each transcription factor between *ApoE*$^{-/-}$ and *Epn1&2-SMC*^{iDKO}*/ApoE*$^{-/-}$ mice. The target genes
345 harboring the differential peaks were used for further signature score calculation in scRNA data.
346
347 **Trajectory Analysis**
348 To calculate the RNA velocity of the single cells, we used the CellRanger output BAM file
349 and GENCODE file to together with the velocyto[31] CLI v.0.17.17 to generate a loom file
350 containing the quantification of spliced and unspliced RNA. Next, we built a manifold,
351 clustered the cells and visualized the RNA velocities using *scVelo*[32]. cytoTRACE analysis with
352 default parameter[33] was performed to predict differentiation states from scRNA-seq data based
353 on the simple yet robust observation that transcriptional diversity decreases during
354 differentiation, to complement the trajectory analysis from RNA velocity. Pseudotime was
355 analyzed using *Monocle* package[34] with reduceDimension and plot_cell_trajectory functions.
356
357 **Cellular Interactions among Different Cell Types**
358 To describe potential cell-to-cell communications, we leveraged the *CellChat* R package[35]
359 to infer the cellular interactions based on the normalized scRNA-seq dataset. The algorithm of
360 CellChat could examine the ligandreceptor interactions significance among different types of
361 cells based on the expression of soluble agonist, soluble antagonist, and stimulatory and
362 inhibitory membrane-bound co-receptors. By summing the probabilities of the ligand-receptor
363 interactions among a given signaling pathway, we could calculate the communication
364 probability for the pathway. In brief, we followed the official workflow and loaded the
365 normalized counts into CellChat and applied the preprocessing functions
366 *identifyOverExpressedGenes*, *identifyOverExpressedInteractions* and *projectData* with
367 standard parameters set. As database we selected the 'Secreted Signaling' pathways and used
368 the pre-compiled 'Protein-Protein-Interactions' as a priori network information. For the main
369 analyses the core functions *computeCommunProb*, *computeCommunProbPathway* and
370 *aggregateNet* were applied using standard parameters and fixed randomization seeds. Finally,
371 to determine the senders and receivers in the network the function *netAnalysis_signalingRole*
372 was applied on the 'netP' data slot.

373
374 **Gene-based Genetic Association Analysis**
375 We used the publicly available GWAS summary statistics of CAD in European
376 populations[36] from a meta-analysis of three datasets, including UK Biobank SOFT CAD
377 GWAS, the CARDIoGRAMplusC4D 1000 Genomes-based GWAS[37], and the Myocardial
378 Infarction Genetics and CARDIoGRAM Exome[38]. The SOFT CAD phenotype in UK
379 Biobank[36] encompasses individuals with fatal or nonfatal myocardial infarction (MI),
380 percutaneous transluminal coronary angioplasty (PTCA) or coronary artery bypass grafting
381 (CABG), chronic ischemic heart disease (IHD) and angina. CARDIoGRAMplusC4D 1000
382 Genomes-based GWAS[37] is a meta-analysis of GWAS studies of mainly European, South
383 Asian, and East Asian, involving 60,801 CAD cases and 123,504 controls. Myocardial
384 Infarction Genetics and CARDIoGRAM Exome[38] is a meta-analysis of Exome-chip studies of
385 European descent involving 42,335 patients and 78,240 controls.
386 A total of 8,908,875 SNPs without exome chip data were retained. We extracted SNPs
387 available in individuals of Utah residents (CEPH) with Northern and Western European
388 ancestry from 1000 Genomes Project (Phase I, version 3), and then performed quality control
389 using the following criteria: minor allele frequency (MAF) > 0.01, call rate ≥ 95% and *P* value
390 of Hardy-Weinberg equilibrium (HWE) > 0.01. Eventually, a total of 7,580,209 SNPs were
391 included for further gene analysis. After variant annotation, SNPs were mapped into 17,910
392 protein-coding genes including the body of the gene or its extended regions (± 20 kb
393 downstream or upstream). The SNP-based *P* values from the GWAS meta-analysis were used
394 as input for the gene-based analysis computed by leveraging a multivariant converging
395 regression model in the Multi-marker Analysis of GenoMic Annotation (MAGMA)[39]. Stringent
396 Bonferroni correction was applied for multiple testing with the genome-wide significance at
397 $P = 2.79E-6$ (0.05/17,910), which generated 68 candidate CAD susceptibility genes for further
398 signature score analysis and pathway enrichment analysis of Gene Ontology by *clusterProfiler*
399 R package.
400
401 **Gene signature score calculation**
402 We calculated signature scores on the basis of scRNA data underlying
403 *PercentageFeatureSet* function in Seurat. CUT&Tag signature score of OCT4 and KLF4 were
404 calculated based on the genes harboring the differential peaks CAD GWAS signature score was
405 calculated based on the expression of 68 CAD susceptibility genes, as well as increased and
406 decreased signature score upon the literature review for 68 genes.
407
408 **Mendelian Randomization**
409 Summary-level statistics of aptamer-based plasma protein KLF4 were extracted from a
410 large-scale protein quantitative trait loci (pQTL) study in 35,559 Icelanders at deCODE. The
411 levels of protein were rank-inverse normal transformed and adjusted for age and sex. Details
412 on the GWAS can be found in the original publication[40]. Mendelian Randomization (MR) is an
413 analytical method, which uses genetic variants as instrumental variables (IVs) to assess the
414 causal effect of specific phenotypes on outcomes[41]. We performed two-sample MR analysis to
415 obtain causal estimates of plasma protein KLF4 on CAD using the *TwoSampleMR* package[42].
416 Independent SNPs (LD $r^2 < 0.001$, within 10,000 kb) at $P < 5e-8$ were retained as instrumental

variables. Inverse-variance-weighted (IVW), weighted median, and MR-Egger regression were primarily used to calculate effect size (β) and corresponding standard error (SE). Heterogeneity was estimated by MR-Egger and IVW methods to assess whether a genetic variant's effect on outcome was proportional to its effect on exposure. Directional pleiotropy was estimated via MR-Egger intercept test for the presence of horizontal pleiotropy.

Statistical Analysis

All wet bench data were expressed as mean ± SEM and the statistical analyses were performed with SPSS 16.0. The 2-tailed Student's *t* test was used for parametric data analyses, ANOVA was used to compare the difference between multiple groups. $P < 0.05$ was considered to be statistically significant.

Results

Upregulated Expression of Epsins in VSMCs in Response to Atherosclerotic Stimuli

To explore whether Epsins in SMCs contribute to the pathogenesis of atherosclerosis, we examined Epsins expressions in atherosclerotic lesions from patients with various disease burdens. In human coronary arteries with disease histologically classified as no lesions, mild lesion with small plaques, and severe lesions with large plaques, we observed that Epsin1 and Epsin2 were expressed in SMCs and in the atherosclerotic lesions. Importantly, the expression of Epsins 1&2 seemed to be enhanced with the increase of the severity of the disease. (Figure S1A).

To evaluate Epsins expression in SMCs in mouse atherosclerotic plaques, we compared Epsins expression in *ApoE*$^{-/-}$ mice fed on normal or western diet for 16 weeks. We found that Epsin1 expression was dramatically increased in the plaques of mice fed on western diet compared to those from mice fed on normal diet (Figure S1B). We next assessed *Epsins* transcript abundance in primary SMCs isolated from *ApoE*$^{-/-}$ mice and found that treatment of SMCs with oxLDL resulted in a 1.9- and 1.7-fold increase in *Epsin1* and *Epsin2* transcripts, respectively (Figure S1C,D). Together, these observations indicated atherosclerotic stimuli increases Epsins expression in SMCs both *in vitro* and in atherosclerotic plaques *in vivo*.

Single-cell Transcriptomics Identified a Novel Cluster of SMC-modulated ECs in the Atherosclerotic Aortae

To determine the role of Epsins in atherosclerosis, we crossed *Epn1*$^{fl/fl}$, *Epn2*$^{-/-}$ mice with *Myh11-iCre*^{ERT2} transgenic mice with a tamoxifen-inducible iCre recombinase knocked into the SMC-specific *Myh11* locus on a bacterial artificial chromosome[26]. We named the resultant *Epn1*$^{fl/fl}$, *Epn2*$^{-/-}$, *Myh11-iCre*^{ERT2} strain as *Epn1&2-SMC*^{iDKO} mice. *Epn1&2-SMC*^{iDKO} mice were further crossed to *ApoE*$^{-/-}$ background (*Epn1&2-SMC*^{iDKO}*/ApoE*$^{-/-}$), injected with tamoxifen to induce the deletion of Epsin1 in SMC (Figure S1E) at the age of 8 weeks, followed by feeding on western diet for 6, 12, and 16 weeks. Immunostaining of aorta sections demonstrated the abrogation of Epsins1&2 in SMCs of aortae from *Epn1&2-SMC*^{iDKO} mice after tamoxifen injection (Figure S1F).

We next performed single-cell RNA sequencing on cells isolated from the whole aortae from *ApoE*$^{-/-}$ *and Epn1&2-SMC*^{iDKO}*/ApoE*$^{-/-}$ mice at baseline and those fed western diet for 6, 12 and 16 weeks (Figure 1A). After stringent quality control of scRNA-seq data processing, a

461 total of 151,944 cells across week feeding groups (Figure S2A,B), i.e., *ApoE*$^{-/-}$: normal diet (n
462 = 23,709), 6-week western diet (n = 6,318), 12-week western diet (n = 27,569), and 16-week
463 western diet (n = 22,258); *Epn1&2-SMC*^{iDKO}*/ApoE*$^{-/-}$: normal diet (n = 16,036), 6-week western
464 diet (n = 21,093), 12-week western diet (n = 15,295), and 16-week western diet (n = 19,666)
465 were retained for downstream analysis. Graph-based clustering of the individual datasets
466 visualized by UMAP[43] and canonical cell marker annotation gave rise to eight main cell
467 clusters (Figure1B, Figure S2C,D), including SMC, modulated SMC (modSMC), modulated
468 SMC with EC markers (modSMC_EC), modulated SMC with fibroblast markers
469 (modSMC_myofibroblast), fibroblast, EC, macrophages, and immune cells.
470 Of particular interest in our scRNAseq result is the emergence of a cell population that
471 retained conventional SMC markers while also expressed the canonical endothelial marker
472 Pecam1 (Figure S2C). As described above, we defined such a cell population as modSMC_EC.
473 It is of note that the abundance of modSMC_EC increased from negligible in normal diet-fed
474 mice aortae to a significant portion in both and *ApoE*$^{-/-}$ and *Epn1&2-SMC*^{iDKO}*/ApoE*$^{-/-}$ mice
475 (Figure 1C, Figure S2E). More importantly, SMC-specific deficiency of Epsins led to increased
476 expression of the conventional EC marker Pecam1 in all cell clusters including modSMC_ECs
477 from aortae of *Epn1&2-SMC*^{iDKO}*/ApoE*$^{-/-}$ mice compared to that from *ApoE*$^{-/-}$ mice (Figure 1D).
478 This observation suggested that atherosclerotic stimuli increased the transition of SMC into
479 modSMC_EC population and Epsins are negative regulators of such a transition. However, the
480 role of the modSMC_ECs which are originated from VSMCs, in the pathogenesis of
481 atherosclerosis is not clear.
482
483 **SMC-intrinsic Epsins Inhibits Transdifferentiation of SMCs into ModSMC_ECs in**
484 **Atherosclerotic Aortae**
485 To investigate the cellular dynamics during the pathological development of
486 atherosclerosis, we performed unsupervised trajectory analysis on the scRNAseq results using
487 RNA velocity algorithms[31]. Cell population trajectory showed little difference between the
488 *ApoE*$^{-/-}$ and *Epn1&2-SMC*^{iDKO}*/ApoE*$^{-/-}$ mice aortae when fed on normal diet. However, such
489 trajectory changed in aortae from mice feed on western diet for 12 or 16 weeks. The velocity
490 flow of VSMCs toward atheroprone macrophages is decreased with concomitant increased
491 VSMC velocity toward modulated SMCs including modSMC_myofibroblast and
492 modSMC_ECs in the aortae of *Epn1&2-SMC*^{iDKO}*/ApoE*$^{-/-}$ mice compared to that in *ApoE*$^{-/-}$
493 mice (Figure 1E). CellRank[44] analysis of the cell dynamics revealed that multiple cell clusters
494 had increased probability to transit into modSMC_EC population in aortae from *Epn1&2-*
495 *SMC*^{iDKO}*/ApoE*$^{-/-}$ mice compared to that in *ApoE*$^{-/-}$ mice (Figure 1F). Taken together with the
496 findings that the proportion of macrophages were drastically decreased in aortae from *Epn1&2-*
497 *SMC*^{iDKO}*/ApoE*$^{-/-}$ mice compared to that in *ApoE*$^{-/-}$ mice fed on western diet (Figure 1B,C),
498 those observations suggest that VSMC-intrinsic Epsins promote the recruitment and
499 accumulation of inflammatory macrophages in atherosclerotic lesions while inhibiting the
500 phenotype transition of VSMCs into athroprotective modSMC_myofibroblast and the
501 modSMC_EC population. As the transition was much more notable in the aortae from mice
502 fed on western diet for 12 and 16 weeks (Figure 1E), with disease progression (Figure S1A,B),
503 we will focus on these groups of mice for the rest of our data analysis.
504 Unsupervised cytoTRACE analysis[33] is used to predicate the cellular differentiation status.

505 Cells with low cytoTRACE score indicated a more differentiated status and vice versa. Similar
506 to the velocity analysis, we observed that the predicted cytoTRACE score of transition from
507 SMC to modSMC relevant cells were significantly lower in *Epn1&2-SMC^{iDKO}/ApoE$^{-/-}$* mice
508 compared with that in *ApoE$^{-/-}$* mice, indicating a higher probability of transition of SMC
509 lineages into modSMC_EC and modSMC_myofibroblsts in the absence of Epsins (Figure 1G).
510 To further investigate the role of Epsins in the transition of SMC into modSMC_ECs, we
511 performed an unsupervised pseudotime analysis[45,46] focusing on the transition from SMC to
512 modSMC_EC. In mice fed on western diet for 16 weeks, modSMC_EC served as an
513 intermediate that tends to be converted back into SMC in the aortae of *ApoE$^{-/-}$* mice as it was
514 located at a tree node at the start of pseudotime. Whereas modSMC_EC in the aortae of
515 *Epn1&2-SMC^{iDKO}/ApoE$^{-/-}$* was at the end of pseudotime derived from SMC, indicating a more
516 differentiated stage toward EC (Figure 1H). Taken together, those scRNAseq data analysis
517 support the conclusion that VSMC-intrinsic Epsins inhibits SMC transition into modSMC_EC
518 under atherosclerotic conditions.
519 Cell-to-cell communications analysis using CellChat[35] revealed increased number and
520 strength of inferred cell-cell interactions in aortae of *Epn1&2-SMC^{iDKO}/ApoE$^{-/-}$* compared to
521 that of *ApoE$^{-/-}$* mice (Figure S3A,B). Among the strengthened communications are the ones
522 involved in the transition of other lineage cells into EC such as VEGF-VEGFR[47], PECAM1
523 (Figure 1I,J), NOTCH1[48] and EGF[49] (Figure S3B-D). To verify those findings in scRNAseq
524 analysis, we performed reverse transcript quantitative PCR (qRT-PCR) and Western blot
525 analysis on homogenates of aortae from tamoxifen injected *ApoE$^{-/-}$* and *Epn1&2-*
526 *SMC^{iDKO}/ApoE$^{-/-}$* mice fed on western diet for 16 weeks. VSMC-specific deficiency of Epsins
527 led to an increase of the EC marker CD31 in aortae from *Epn1&2-SMC^{iDKO}/ApoE$^{-/-}$* mice
528 compared to that from *ApoE$^{-/-}$* mice (Figure S3E, Figure 3A). We concluded that Epsins in the
529 VSMCs inhibits signaling flow between cells that promotes the transition of SMCs into
530 endothelial-like cells.
531
532 **SMC-intrinsic Epsins Promoted Atherosclerosis through Destabilizing SMCs'**
533 **Contractile Phenotype**
534 We next performed Gene Ontology pathway enrichment of differentially expressed genes
535 in SMCs from aortae from *ApoE$^{-/-}$* and *Epn1&2-SMC^{iDKO}/ApoE$^{-/-}$* mice across normal diet and
536 western diet-fed (Table S5), and notably observed that the presumably atheroprone signaling
537 pathways such as TLR[50], ERK[51], PI3K[52], TGFβ[20], NF-κB[53] were decreased in aortae from
538 *Epn1&2-SMC^{iDKO}/ApoE$^{-/-}$* mice compared to that from *ApoE$^{-/-}$* mice (Figure 2A). In addition to
539 the compromised atheroprone pathways, cholesterol storage and foam cell differentiation were
540 also decreased in Epsins-deficient VSMCs, suggesting that Epsins in VSMC promoted
541 cholesterol accumulation and foam cell formation which promotes the formation and growth
542 of atherosclerotic plaques. Moreover, Epsins in VSMC promoted the activation of
543 proinflammatory cells and cytokinesis production. All these data underpin an atheroprone role
544 of Epsins in VSMCs that underlies the pathogenesis of atherosclerosis。
545 To explore the relevance of our mice scRNAseq data to human diseases, we retrieved 68
546 CAD signature genes identified through GWAS analysis in European populations[36] (Figure
547 S4A, Table S3) and mapped the transcript abundance of those genes in our scRNAseq dataset.
548 Overall, the expression of the 68 CAD signature genes are significantly lower in cells across

549 all the population in aortae of *Epn1&2-SMC^{iDKO}/ApoE$^{-/-}$* that that from *ApoE$^{-/-}$* mice (Figure
550 S4B). Notably, 19 of 68 CAD genes are associated with increased CAD risk, while 30 are
551 associated with decreased CAD risk (Table S3) in the GWAS dataset. Intriguingly, we observed
552 that the 19-gene cohort associated with increased CAD risk are downregulated in multiple cell
553 types from the aortae of *Epn1&2-SMC^{iDKO}/ApoE$^{-/-}$* mice compared to that from *ApoE$^{-/-}$* mice
554 (Figure 2B), while no significant differential expression were found in the 30-gene cohort
555 associated with decreased CAD risk among the two genotypes (Figure S4C).
556 We next performed pathway enrichment analysis on the 68 CAD signature genes (Table
557 S4). We observed the enrichment of several atheroprone biological process pathways such as
558 PI3K, MAPK, WNT, and STAT, as well as pathways involving inflammatory immune
559 responses and affecting cell phenotypes and functions (e.g., SMC proliferation, EC migration,
560 and vascular permeability) (Figure 2C). Intriguingly, those presumably atheroprone pathways
561 such as PI3K[52], MAPK[54], WNT[55], and STAT[56], inflammatory immune responses, and cellular
562 function and biology were also identified in pathway enrichment assay using the differentially
563 expressed genes of our scRNAseq results of mouse aortae (Figure 2C). More importantly, those
564 presumably atheroprone pathways are downregulated in aortae SMCs from *Epn1&2-*
565 *SMC^{iDKO}/ApoE$^{-/-}$* mice compared to that from *ApoE$^{-/-}$* mice. Together, combining the GWAS
566 of human data and our scRNAseq data, we conclude that VSMC-intrinsic Epsins are
567 atheroprone.
568 To explore the mechanism by which Epsins contribute to the pathology of atherosclerosis
569 as suggested by combined data of scRNAseq and GWAS, we harvested aortae from tamoxifen
570 injected *ApoE$^{-/-}$* and *Epn1&2-SMC^{iDKO}/ApoE$^{-/-}$* mice fed on western diet for 16 weeks. qRT-
571 PCR analysis showed that the expression of VSMC markers related to VSMC contractile
572 phenotype (i.e., *Acta2*, *Cnn1*, *Tagln*, and *Myh11*)[8] were significantly higher in the aortae from
573 *Epn1&2-SMC^{iDKO}/ApoE$^{-/-}$* mice than that from *ApoE$^{-/-}$* mice (Figure S5A). Western blot on
574 aortae homogenates and immunostaining on aortae sections further showed that VSMC-
575 specific deficiency of Epsins led to stabilization of SMC contractile markers, as well as a
576 decrease of macrophage marker Galectin3 in aortae from *Epn1&2-SMC^{iDKO}/ApoE$^{-/-}$* mice
577 compared to that from *ApoE$^{-/-}$* mice (Figure 2D,E). To track VSMC phenotypic switching in
578 atherogenesis, we crossed *Epn1&2-SMC^{iDKO}/ApoE$^{-/-}$* mice with Rosa26Stop-floxed eYFP
579 reporter stain of mice[57] generating in *Epn1&2-SMC^{iDKO}/eYFP$^{+/-}$/ApoE$^{-/-}$* compound mutant
580 mice (Figure S5B). When those mice were injected with tamoxifen at the age of 8 weeks, all
581 SMCs and cells derived from SMCs subsequently will be permanently labelled with eYFP. In
582 brachiocephalic trunk sections of 16-week western diet-fed mice, there were less eYFP^{+}
583 Lgals3^{+} macrophages and Ecrg4^{+} fibroblasts localized in the media of the lesions from
584 *Epn1&2-SMC^{iDKO}/eYFP$^{+/-}$/ApoE$^{-/-}$* mice compared to that from *eYFP$^{+/-}$/ApoE$^{-/-}$* mice (Figure
585 2F,G). Meanwhile, significantly more Ecrg4^{+} eYFP^{+} modSMC_myofibroblasts cells were
586 found localized in intima overlying the media in *Epn1&2-SMC^{iDKO}/eYFP$^{+/-}$/ApoE$^{-/-}$* mice
587 compared to that of *eYFP$^{+/-}$/ApoE$^{-/-}$* mice (Figure 2G), indicating that modSMC_myofibroblast
588 preferentially localized into the fibrous cap in the atherosclerotic lesions from *Epn1&2-*
589 *SMC^{iDKO}/eYFP$^{+/-}$/ApoE$^{-/-}$* mice. To explore the role of Epsins in the VSMC phenotype
590 switching under atherosclerotic challenges in vitro, aortic VSMCs isolated from *ApoE$^{-/-}$* mice
591 and tamoxifen injected *Epn1&2-SMC^{iDKO}/ApoE$^{-/-}$* mice were treated with 100 μg/mL oxLDL
592 for 72 hrs, followed by western blot. oxLDL treatment led to decreased expression of VSMC

593 contractile makers and such decrease was not as significant in Epsins-deficient VSMCs as that
594 from *ApoE*$^{-/-}$ mice (Figure S5C). Taken together the scRNAseq and biochemical results, we
595 conclude that VSMC-intrinsic Epsins destabilized the contractile phenotypes of VSMCs.
596
597 **ModSMC_EC Cells were Functional and Participate in the Repair of Endothelial Injury**
598 **Caused by Atherosclerosis.**
599 Flow cytometry of total cells dissociated from aortae indicated that there were higher
600 proportion of CD31^{+}, eYFP^{+} modSMC_EC in total cells from aortae of *Epn1&2-*
601 *SMC*^{iDKO}*/eYFP*$^{+/-}$*/ApoE*$^{-/-}$ mice compared to that from *eYFP*$^{+/-}$*/ApoE*$^{-/-}$ mice (Figure 3B).
602 Immunostaining of atherosclerotic brachiocephalic trunk sections from *Epn1&2-*
603 *SMC*^{iDKO}*/eYFP*$^{+/-}$*/ApoE*$^{-/-}$and *eYFP*$^{+/-}$*/ApoE*$^{-/-}$ mice showed a significantly more CD31^{+} (Figure
604 3D) or VE-Cadherin^{+} (Figure 3E) cells that were also eYFP^{+} in *Epn1&2-SMC*^{iDKO}*/eYFP*$^{+/-}$
605 */ApoE*$^{-/-}$ mice compared to that from *eYFP*$^{+/-}$*/ApoE*$^{-/-}$ mice. More importantly, we observed that
606 those CD31, or VE-Cadherin and eYFP double positive cells (modSMC_ECs) were localized
607 in the endothelial layer of blood vessel (Figure 3C-F). Those observations suggested that
608 indeed SMCs can transdifferentiate into endothelial-like cells in atherosclerotic arteries and
609 absence of Epsins promoted such switching. To explore whether Epsins deficiency promotes
610 SMCs to modSMC_EC phenotype switching *in vitro*, we immunostained primary aortic SMCs
611 in long-term culture with αSMA and endothelial markers. Epsins-deficient SMCs showed
612 increased expression of both CD31 and NRP1 compared to wild-type SMCs (Figure S5D).
613 Taken together, those observations suggest that absence of Epsins in SMC promotes the
614 transition of SMC into modSMC_EC and such modSMC_ECs may participate in the repair of
615 EC damages caused by atherosclerotic stimuli.
616 One of the fundamental functions of ECs is endocytosis of ac-LDL which helps
617 maintaining homeostasis of blood cholesterol level[58]. Thus, we evaluated whether
618 modSMC_ECs in atherosclerotic plaques can take up ac-LDL. We sorted eYFP^{+} cells from
619 total cells freshly dissociated from the aortae of *eYFP*$^{+/-}$*/ApoE*$^{-/-}$ and *Epn1&2-SMC*^{iDKO}*/eYFP*$^{+/-}$
620 */ApoE*$^{-/-}$ mice fed on western diet for 14 weeks. The sorted eYFP^{+} cells were treated with Dil-
621 ac-LDL[59] for 5 hrs followed by immunostaining with endothelial markers CD31 or VE-
622 Cadherin. There were increased proportion of eYFP^{+} cells that took up ac-LDL, and the
623 proportion of eYFP and CD31 or VE-Cadherin double positive modSMC_ECs were also
624 increased in cells isolated from aortae of *Epn1&2-SMC*^{iDKO}*/eYFP*$^{+/-}$*/ApoE*$^{-/-}$ mice compared to
625 that from *eYFP*$^{+/-}$*/ApoE*$^{-/-}$. Moreover, there were higher number of Epsins-deficient
626 modSMC_ECs that took up ac-LDL compared to wild-type control modSMC_ECs (Figure 3H-
627 J). Furthermore, each Epsins-deficient modSMC_EC took up more ac-LDL in culture
628 compared to that from wild-type controls (Figure 3K). Western blot revealed that knockdown
629 of Epsins in cultured SMCs lead to increaed expression of CD31 proteins upon oxLDL
630 stimulation (Figure 3L) corroborating earlier findings that Epsins negatively regulate SMC to
631 modSMC_EC transition. Taken together, these data suggest that Epsins deficiency promotes
632 SMCs transdifferentiating to modSMC_ECs and these SMC-originated endothelial-like cells
633 were functional in ingestion of ac-LDL. ModSMC_ECs can integrate into the arterial vessel
634 wall and likely to participate in the repair of atherosclerosis-induced endothelial damage.
635
636 **Epsins Suppress the Expression of SMC Markers by Decreasing KLF4 Expression**

637 KLF4 is a critical regulator of SMC phenotypic modulation[7,60-62]. Considering the
638 enrichment of KLF4 in extracellular space evidenced by GeneCards
639 (https://www.genecards.org/cgi-bin/carddisp.pl?gene=KLF4#localization), we performed a
640 Mendelian Randomization analysis to evaluate the relationship between KLF4 and CAD risk
641 (Figure S4A), and observed that higher level of plasma KLF4 protein was causally associated
642 with increased risk of CAD in the general population (β = 0.18, P = 0.035; Figure 4A). We
643 further observed that KLF4 colocalizes with SMC marker αSMA in atherosclerotic human
644 aortae and the amount of KLF4 protein increased with the advancement of atherosclerosis
645 (Figure 4B). This observation suggests that KLF4 level is increased in SMCs with the
646 progression of atherosclerosis.
647 Western blot of homogenates of aortae from mice fed on normal or western diet
648 recapitulated the increased expression of KLF4 in atherosclerotic lesions as that observed in
649 human samples (Figure 4C, Figure S6A). Interestingly, such upregulation was almost
650 abrogated in aortae from *Epn1&2-SMC*^{iDKO}*/ApoE*$^{-/-}$ mice compared to that from *ApoE*$^{-/-}$ mice
651 (Figure 4D,E, Figure S6B). This difference was not due to lower KLF4 mRNA transcript
652 abundance in Epsins-deficient aortae, suggesting a post-transcriptional regulation of KLF4
653 stability by Epsins (Figure S6C). In addition, we sorted SMCs from aortae of 16-week western
654 diet-fed eYFP-tagged SMC-lineage tracing mice and determined the expression of KLF4 by
655 immunostaining. Both flow cytometric analyses and confocal microscopy showed that about
656 90.1% of eYFP^{+} SMCs from *eYFP*$^{+/-}$*/ApoE*$^{-/-}$ mice are positive for KLF4. Whereas only 66.5%
657 of eYFP^{+} SMCs from aortae of *Epn1&2-SMC*^{iDKO}*/eYFP*$^{+/-}$*/ApoE*$^{-/-}$ mice were positive for
658 KLF4. Moreover, the KLF4 expression level is lower in eYFP^{+} SMCs from *Epn1&2-*
659 *SMC*^{iDKO}*/eYFP*$^{+/-}$*/ApoE*$^{-/-}$ mice than that from *eYFP*$^{+/-}$*/ApoE*$^{-/-}$ mice (Figure 4F,G, Figure S6D).
660 We further stimulated SMCs isolated for mouse aortae from mice on normal diet with
661 scrambled or Epsins siRNAs followed by oxLDL. oxLDL treatment induced the upregulation
662 of KLF4 in vitro in SMCs pretreated with scrambled RNA (Figure 4I, Figure S6E). However,
663 both the basal level and oxLDL-induced upregulation of KLF4 were reduced in the absence of
664 Epsins in primary SMC (Figure 4I, Figure S6E). Similarly, immunofluorescence staining
665 showed that KLF4 proteins in primary SMCs were less abundant in SMCs from *Epn1&2-*
666 *SMC*^{iDKO}*/ApoE*$^{-/-}$ mice compared to that from *ApoE*$^{-/-}$ mice after oxLDL treatment (Figure S6F).
667 These data indicated that Epsins were crucial for stabilizing the protein level of KLF4 in SMCs.
668 To further explore whether KLF4 is downstream of Epsins in modulating SMC phenotypic
669 modulation, we performed CUT&Tag profiling[30] against KLF4 in SMCs isolated from aortae
670 of *ApoE*$^{-/-}$ and *Epn1&2-SMC*^{iDKO}*/ApoE*$^{-/-}$ mice fed on western diet for 16 weeks. After
671 comparing differential binding peaks between the two genotypes, we retrieved 1113 target
672 genes from KLF4 Cut&Tag array and mapped them to scRNAseq dataset as KLF4 binding
673 gene signature (Table S5). Intriguingly, we observed that the KLF4 binding gene signature
674 score was lower in SMC from *Epn1&2-SMC*^{iDKO}*/ApoE*$^{-/-}$ mice than that from *ApoE*$^{-/-}$ mice
675 (Figure 4H), especially in cell types of SMC, modSMC_EC, modSMC_myofibroblasts, and
676 macrophage cells (Figure S6G). In parallel, we determined the expression pattern of SMC
677 markers in SMCs from *Epn1&2-SMC*^{iDKO}*/ApoE*$^{-/-}$ mice after adenovirus-mediated
678 overexpression of KLF4 and observed that SMC markers *Tagln* and *Acta2* were dramatically
679 inhibited upon KLF4 over-expression (Figure S6H). Together, these findings suggest that
680 Epsins promotes SMC phenotype switching in atherosclerosis through increasing KLF4 protein

681 abundance.
682
683 **Epsins Binds Directly to KLF4 and Prevent its Ubiquitination and Subsequent**
684 **Degradation**
685 To explore the molecular mechanisms how Epsins increases the protein abundance of
686 KLF4 in SMCs in atherosclerotic lesions, we performed coimmunoprecipitations from lysates
687 of primary SMCs isolated from *ApoE*$^{-/-}$ mice treated with siRNAs to induce the deletion of
688 Epsins followed by oxLDL stimulation. As shown in Figure 4I, we observed a basal binding of
689 KLF4 to Epsin1 in unstimulated SMCs, which was increased in response to oxLDL treatment
690 (Figure 4I,J). KLF4 can be degraded by the ubiquitination-proteosome pathway[63]. To
691 determine whether Epsins control KLF4 stability in SMCs in atherosclerosis through the
692 ubiquitination-proteosome pathway, we transfected SMCs with scrambled and siRNAs against
693 Epsins1&2 followed by treatment with 100 nM proteasome inhibitor MG132 for 6 hrs. Cells
694 were then stimulated with 100 μg/mL oxLDL for 24 hrs. Immunoprecipitation-western showed
695 that Epsins depletion led to decreased KLF4 protein level. oxLDL treatment caused
696 polyubiquitination of KLF4 and such ubiquitination was enhanced upon depletion of Epsins.
697 More importantly, inhibition of proteosome activity increased the protein level of KLF4 in
698 Epsins-depleted SMCs (Figure 4K, Figure S6I,J). Together, those observations suggest that
699 Epsins stabilize KLF4 through inhibiting its ubiquitination and subsequent proteosome-
700 mediated degradation.
701 We have previously shown that Epsins could recognize ubiquitinated proteins via its
702 ubiquitin-interacting motif (UIM)[21,22]. To determine which Epsins domains are responsible for
703 the interaction with KLF4, we created mammalian expression vectors containing cDNAs
704 encoding HA-tagged full length, ENTH domain, UIM, or ENTH+UIM deletion Epsin1 (HA-
705 Epsin1^{WT}, HA-Epsin1$^{\triangle ENTH}$, HA-Epsin1$^{\triangle UIM}$ or HA-Epsin1$^{DPW/NPF}$). We transfected these
706 constructs to HEK 293T cells together with a plasmid expressing KLF4. We performed
707 immunoprecipitation on cell lysates with anti-HA antibody and western blot showed that both
708 ENTH and UIM domain of Epsin1 played a role in the interaction between Epsin1 and KLF4
709 as the binding between Epsin1$^{\triangle UIM/\triangle ENTH}$ and KLF4 was declined, meanwhile, the binding
710 between Epsin1$^{DPW/NPF}$ and KLF4 was abrogated (Figure 4L, Figure S6K). Taken together,
711 Epsins stabilize KLF4 by binding to KLF4 through its ENTH and UIM domain.
712 KLF4 ubiquitination is catalyzed by VHL, an E3 ubiquitin ligase, for proteasomal
713 degradation, in breast carcinoma cells[64]. We hypothesize that Epsins inhibits KLF4
714 ubiquitination by interfering with the interaction between VHL and KLF4. Firstly, scRNAseq
715 data showed that both *Vhl* and *Klf4* expressions in SMC from *Epn1&2-SMC*^{iDKO}*/ApoE*$^{-/-}$ mice
716 fed on western diet were significantly increased (Figure S7A). Immunostaining of human aorta
717 sections containing atherosclerotic lesions showed that VHL level in αSMA-positive SMCs
718 correlated strongly with increased disease severity (Figure S7B). To determine whether Epsins
719 interfere with the interaction between VHL and KLF4, we performed co-immunoprecipitation
720 assays in wild-type and Epsins-deficient SMCs using VHL-specific antibody. Epsins
721 deficiency increased VHL protein level in SMCs (Figure S7C,D), and significantly enhanced
722 the interaction between VHL and KLF4 regardless of the presence of oxLDL (Figure S7C,E).
723 Together, those data suggest that loss of Epsins reduced KLF4 expression by interfering with
724 the interaction between VHL and KLF4.

725

726 **Epsins Inhibit the Expression of EC Markers in SMCs by Destabilizing OCT4**

727 Given the critical role of OCT4 in controlling the plasticity of SMCs in atherosclerosis[18],
728 we investigated whether SMC Epsins control OCT4 activity in this process. We have enriched
729 OCT4 binding genes derived from CUT&Tag array (Table S6) and found that OCT4 binding
730 gene signature score in both SMC and modSMC_EC was significantly higher in SMCs from
731 atherosclerotic aortae of *Epn1&2-SMC*^{iDKO}*/ApoE*$^{-/-}$ mice than that from *ApoE*$^{-/-}$ mice (Figure
732 5A). Consistently, OCT4 protein level was higher in the homogenate of aorta from *Epn1&2-*
733 *SMC*^{iDKO}*/ApoE*$^{-/-}$ mice compared to that from *ApoE*$^{-/-}$ mice, interestingly, we also observed that
734 the RNA level of Oct4 were also upregulated in SMCs isolated from *Epn1&2-SMC*^{iDKO}*/ApoE*$^{-}$
735 $^{/-}$ mice (Figure 5B,C). Furthermore, the increased level of OCT4 protein was observed in aortic
736 arch, thoracic aortae and abdominal aortae from *Epn1&2-SMC*^{iDKO}*/ApoE*$^{-/-}$ mice compared
737 with *ApoE*$^{-/-}$ mice (Figure 5D). Immunostaining of brachiocephalic trunk from mice fed on
738 western diet for 16 weeks showed that OCT4 was readily detected in the brachiocephalic trunk
739 from *Epn1&2-SMC*^{iDKO}*/ApoE*$^{-/-}$ with little detected in brachiocephalic trunk from *ApoE*$^{-/-}$ mice
740 and OCT4 co-localized with αSMA (Figure S8A,B). We speculated that Epsins negatively
741 regulate OCT4 protein level regardless of atherosclerotic stimuli. Indeed, the expression of
742 OCT4 in Epsins-knockdown primary SMCs was higher than that in scramble RNA control
743 SMCs regardless of oxLDL treatment (Figure 5E).

744 To explore the role of OCT4 in SMC phenotype modulation, we immunostained
745 brachiocephalic trunk sections from *eYFP*$^{+/-}$*/ApoE*$^{-/-}$ and *Epn1&2-SMC*^{iDKO}*/eYFP*$^{+/-}$*/ApoE*$^{-/-}$
746 mice with anti-CD31 and OCT4 antibodies. OCT4 expressed highly in eYFP^{+} CD31^{+} cells
747 localized in the intima of plaque of brachiocephalic trunk from *Epns-SMC*^{iDKO}*/eYFP*$^{+/-}$*/ApoE*$^{-}$
748 $^{/-}$ mice (Figure 5F). To corroborate those immunostaining findings, we dissociated aortae cells
749 and stained with anti-VE-cadherin and observed that about 2.71% of eYFP^{+} SMCs were OCT4
750 and VE-cadherin double positive in *Epn1&2-SMC*^{iDKO}*/eYFP*$^{+/-}$*/ApoE*$^{-/-}$ mice, whereas only
751 0.63% were found in brachiocephalic trunk from *eYFP*$^{+/-}$*/ApoE*$^{-/-}$ mice (Figure 5G). In addition,
752 we sorted eYFP-positive cells from SMC-lineage tracing mice fed on western diet for 16 weeks
753 and stained with CD31/VE-Cadherin and OCT4. There were more OCT4^{+} CD31^{+} and OCT4^{+}
754 VE-Caherin^{+} eYFP-tagged cells from *Epn1&2-SMC*^{iDKO}*/eYFP*$^{+/-}$*/ApoE*$^{-/-}$ than that from
755 *eYFP*$^{+/-}$*/ApoE*$^{-/-}$ mice (Figure 5H,I Figure S8C). Taken together, OCT4 preferentially localized
756 in EC marker-positive modSMC_ECs suggesting that OCT4 may play a role in SMC to
757 modSMC_EC modulation.

758 To further explore whether OCT4 is downstream of Epsins to suppress the expression of
759 SMC contractile markers as well as SMC to endothelial transdifferentiation, we performed both
760 qRT-PCR and western blot in SMCs isolated from *Epn1&2-SMC*^{iDKO}*/ApoE*$^{-/-}$ mice treated with
761 tamoxifen and OCT4 siRNA. Knocking down of *Oct4* in Epsins-deficient SMC led to decrease
762 of SMC contractile markers as well as EC marker CD31 (Figure S8D,E).

763

764 **SMC-Specific Epsins Deficiency Reduced the Size of Atherosclerotic Lesion and**
765 **Increased the Plaque Stability in *vivo*.**

766 Given our observation that Epsins expression was upregulated in SMC in atherosclerotic
767 lesions and SMC-specific Epsins deficiency selectively increase SMC transition to endothelial-
768 like cells which in turn participate in the repair of endothelial injury caused by atherogenic

769 stimuli, we speculated that Epsins deficiency in SMC would improve the outcome of
770 experimental atherosclerosis *in vivo*. To test this, *ApoE*$^{-/-}$ mice and tamoxifen injected *Epn1&2-*
771 *SMC*^{iDKO}*/ApoE*$^{-/-}$ mice were fed a western diet for 9, 16, 20 weeks. Assessment of the *en face*
772 lesion area in whole aorta revealed that atherosclerotic lesion was significantly smaller in
773 *Epn1&2-SMC*^{iDKO}*/ApoE*$^{-/-}$ mice compared to *ApoE*$^{-/-}$ mice (P = 0.0012 with 9-week western
774 diet, P = 0.0247 with 16-week western diet, P = 0.0003 with 20-week western diet, compared
775 with control *ApoE*$^{-/-}$ mice; Figure 6A). Furthermore, examination of aortic root lesions
776 demonstrated that tamoxifen injected *Epn1&2-SMC*^{iDKO}*/ApoE*$^{-/-}$ mice had a 56.57% reduction
777 in lesion area in comparison to *ApoE*$^{-/-}$ mice (Figure 6B,C). Using Oil Red O staining, we also
778 observed significant reduction in lipid loading in the lesion of sinus and brachiocephalic trunk
779 in *Epn1&2-SMC*^{iDKO}*/ApoE*$^{-/-}$ mice compared to *ApoE*$^{-/-}$ mice (Figure 6D,E).
780 To evaluate the inflammatory profile of the atherosclerotic lesions of these mice, we
781 assessed lesion composition by immunostaining with markers of macrophages (CD68) within
782 aortic sinus lesions. Consistent with a reduction in atherosclerotic progression, we detected a
783 reduction in macrophage area by 59.2% in tamoxifen injected *Epn1&2-SMC*^{iDKO}*/ApoE*$^{-/-}$ mice
784 (P < 0.0001 vs *ApoE*$^{-/-}$ mice; Figure 6F). Last, we observed a reduction in ICAM-1 and P-
785 selectin staining in the endothelial layer of aortic root lesions of tamoxifen injected *Epn1&2-*
786 *SMC*^{iDKO}*/ApoE*$^{-/-}$ mice compared to *ApoE*$^{-/-}$ mice (Figure 6G-H), which was consistent with the
787 reduced recruitment and accumulation of macrophages in the atherosclerotic plaques of these
788 mice. Together, these data demonstrated that deficiency of Epsin1&2 in SMC could protect
789 against atherosclerotic progression induced by a western diet.
790 In addition to reduction of lesion size, a thick fibrous cap as well as a smaller necrotic core
791 are important features of stable plaques that are less likely to be disrupted to cause thrombosis[65].
792 Our scRNAseq results showed that loss of *Epsin1&2* in SMCs increased the SMC-derived
793 myofibroblasts which is beneficial to the protective fibrous cap formation[12] (Figure 1D, Figure
794 S2D). Deficiency of Epsins in SMC also led to increased thickness of the fibrous cap of
795 atherosclerotic lesions in *Epn1&2-SMC*^{iDKO}*/ApoE*$^{-/-}$ mice compared to that in *ApoE*$^{-/-}$ mice fed
796 on western diet (Figure 2E) To assess plaque stability, we analyzed the size of necrotic core,
797 plaque collagen content, accumulation of contractile SMC content and dead cell content.
798 Epsins specific knockout in SMCs: 1) significantly reduced the necrotic core area to total
799 plaque area ratio as determined by hematoxylin and eosin staining (Figure 6I), 2) markedly
800 elevated the total plaque collagen content as determined by Van Gieson's staining (Figure 6J),
801 and 3) significantly decreased the dead cell content which was marked by cleaved-Caspase3
802 (Figure 6K) in atherosclerotic lesions.
803
804 **Discussion**
805 Our previous studies have elucidated an atheroprone function of Epsins in both ECs[20,21],
806 and macrophages[22,66] in the pathogenesis of atherosclerosis. However, as the major source of
807 plaque cells and extracellular matrix (ECM) at all stages of atherosclerosis, the role of SMC-
808 intrinsic Epsins in pathogenesis of atherosclerosis remains largely unknown. By integrating
809 scRNAseq data with GWAS, we discovered that Epsins-deficiency specifically in VSMCs led
810 to suppressed expression of genes associated with increased CAD risks, highlighting the pivotal
811 role of VSMC-intrinsic Epsins in the pathological process leading to CAD. Using single-cell
812 genomics and mouse strains with VSMC-specific Epsins deficiency and lineage tracing, we

813 revealed VSMCs can transdifferentiate into endothelial-like cells. Specifically, loss of Epsins
814 results in a higher proportion of SMC-derived endothelial-like cells and myofibroblasts,
815 particularly in advanced atherosclerotic lesions. While the SMC-derived endothelial-like cells
816 may participate in the repair of endothelial damage, the myofibroblasts transdifferentiated from
817 SMCs stabilizes atherosclerotitc plaque cap. Both cell types are athero-protective. Therefore,
818 the SMC-intrinsic Epsins promote the pathogenesis of atherosclerosis at least in part through
819 inhibition of phenotype switching of SMCs into athero-protective cell types.
820 Using single-cell genomics and mouse strains with SMC-specific Epsins deficiency and
821 lineage tracing, we revealed SMCs can transdifferentiate into endothelial-like cells.
822 Specifically, loss of Epsins results in a higher proportion of SMC-derived endothelial-like cells
823 and myofibroblasts, particularly in advanced atherosclerotic lesions. Previous studies reported
824 SMC-derived *Vcam*$^{+}$ cells, which were assumed to be SEMs (stem cell, endothelial cell and
825 monocytes/macrophage differentiation, termed de-differentiated SMCs) defined as an
826 intermediate cell state, in human atherosclerotic plaques and mouse atherosclerotic models[13].
827 Of greatest significance, through a series of trajectory analyses of our scRNAseq data, we show
828 that the absence of Epsins not only increase the transition from SMC to modSMC_EC, but also
829 stabilized SMC-derived endothelial-like cell population. Harnessing a lineage tracing mice, in
830 combination with flow cytometry cell sorting and endothelial functional assessment, as well as
831 confocal microscopy of aortae sections, we revealed that SMC-derived endothelial-like cells
832 showed basic EC functions and may integrate into vascular vessel wall to participate the
833 reparation of endothelial injury caused by atherosclerotic stimuli. Taken together, our studies
834 suggest that the molecular features of SMC-derived endothelial-like cells represent a unique
835 transitional state from SMCs to endothelial-like cells in the milieu of atherosclerosis. Epsins'
836 deficiency enhanced the conversion of SMCs into such SMC-derived endothelial-like cells.
837 Anatomically, there are multiple layers of SMCs whereas there is only one single layer of
838 endothelial cell in arterial wall. This is reflected by the scRNAseq data that SMC is the largest
839 population while ECs is a minor one. Despite the fact that the proportion of modSMC_EC is
840 low among the whole modulated SMC-derived cell population, those modSMC_ECs are
841 located in the vicinity of damaged endothelial cells. Therefore, those small number of
842 modSMC_ECs play a pivotal role in the repair of injured arterial endothelial wall. The
843 mechanisms why modSMC_ECs are mostly located near arterial injury sites deserves further
844 investigation.
845 In the current study, Mendelian Randomization analysis showed that the elevated plasma
846 KLF4 protein constitute as a risk factor of CAD in the general population. Consistently, KLF4
847 in SMCs was abundant in both human and mouse atherosclerotic lesions which correlated with
848 the upregulation of Epsins. More importantly, the upregulation of KLF4 in response to
849 atherogenic stimuli was attenuated in the absence of Epsins. Given Epsins' classical role as a
850 membrane-associated endocytic adaptor, they are unlikely to regulate *KLF4* at the
851 transcriptional level. It has been reported previously that once KLF4 is expelled from the
852 nuclear, it is quickly ubiquitinated followed by proteosome-mediated degradation in mouse
853 blastocysts[67]. In the absence of Epsins, both KLF4 expression level and nuclei localization
854 were reduced in oxLDL treated SMCs, suggesting that Epsins are critical for maintaining KLF4
855 protein level. In contractile SMCs, KLF4 protein level is kept in check by VHL ubiquitin E3
856 ligase which serve to prevent the conversion of those cells into synthetic phenotypes[68]. Our

current data supports a model in which Epsins interacts constitutively with KLF4 via its UIM and ENTH domains, interfering with KLF4-VHL interaction, thus reducing KLF4 ubiquitination and degradation.

KLF4 as a transcription factor has been implicated in SMC phenotype modulation[7,69]. In our study, we showed that phenotypically modulated SMCs transdifferentiate to multiple phenotypes, including cells that express markers of myofibroblast, macrophage, and EC in a mouse model of atherosclerosis. Forced ectopic expression of KLF4 in Epsins-deficient SMCs induced a marked reduction in SMCs contractile phenotype, while it had no effect on endothelial-like SMC phenotype. However, the role of KLF4 in regulation of gene expression and coordination with other transcriptions factors is context-dependent[60,70,71]. In addition to transcriptional regulation, KLF4 functions as a scaffolding protein to recruit other transcriptional regulators to promoters of SMC marker genes in response to different environmental cues[72]. KLF4/OCT4 complex is sufficient and necessary to generate induced pluripotent stem cells from several cell types, such as dermal papilla cells and adult neural stem cells[73, 74,75]. However, previous studies have shown that loss of OCT4 within SMC had virtually completely opposite overall effects on lesion pathogenesis as compared to SMC specific loss of KLF4[15]. In our current study, knockdown of OCT4 in SMCs resulted in reduced SMC markers and EC marker expression. Our data supported that KLF4 and OCT4 controls opposite aspects of SMC phenotypic transitions in the atherosclerotic context[7,18]. It remains unclear how KLF4 and OCT4 coordinate to control the transdifferentiaton of VSMCs. It has been shown that KLF4 can bind to the promoter region of OCT4 and enhance OCT4 transcription[18]. Nevertheless, we found that SMC Epsins deficiency led to decreased KLF4 but increased OCT4 protein level in SMC-derived endothelial-like cells. Though OCT4 expression was hardly detectable in the aorta of the *ApoE*$^{-/-}$ control mice which is in line with earlier findings that Oct4 is barely detectable in most adult mouse organs[76], nevertheless, OCT4 protein level was increased dramatically in aortae from Epsins-deficient mice. The underlying molecular mechanisms by which Epsins control the protein level of Oct4 merits further investigation in relation to KLF4 level. In addition, future studies are warranted to comprehensively evaluate the predictive value of the therapeutic effects of targeting VSMC Epsins with siRNA nanoparticles to halt atherosclerosis progression.

In this study, we discovered that the expression level of Epsins in SMCs tightly correlated with the severity of the disease in both human and mouse atherosclerotic aortae. Notably, selective loss of *Epsin1 and 2* within SMCs led to 1) reduced lesion size and lipid load, 2) enhanced stability of the plaque, including increased fibrous cap thickness and decreased necrotic core, 3) reduced proinflammatory macrophage and the number of dead cells in the necrotic core, 4) increased *Myh11*$^{+}$ and *Acta2*$^{+}$ cells within the fibrous cap. Taken together our discovery that Epsins differentially control the protein level of KLF4 and OCT4 in aortic SMCs, and previously established disparate role of Klf4 and Oct4 in the pathogenesis of atherosclerosis[7,18,19] support our findings, an atheroprone function of SMC Epsins.

In summary, our study reveals a novel cell state during SMC phenotypic switching and identifies potential therapeutic targets to repair the dysfunctional endothelium in atherosclerosis. Epsins are critical for SMC dedifferentiation in atherosclerosis disease progression by protecting KLF4 from ubiquitination and proteasomal degradation. The absence of Epsins in SMCs resulted in the loss of KLF4 and hampered the progression of atherosclerosis

in *Epn1&2-SMC^{iDKO}/ApoE$^{-/-}$* mice. These insights may pave the way for targeted SMC-Epsins inhibition as a novel therapeutic treatment of CAD.

Acknowledgments

We thank the Flow Cytometry Core at Boston Children's Hospital for the use of the LSRII, BGI Hong Kong for the scRNA-sequencing, and the Biopolymers Facility at Harvard Medical School for quality control analysis of RNA samples. Dr. John Shyy from University of California, San Diego provided KLF4 AAV construct. Dr. Gary K. Owens from University of Virginia provided Rosa26Stop-floxed eYFP reporter stain of mice. Xinlei Gao and Kaifu Chen from Boston Children's Hospital/Harvard Medical School provided bioinformatic suggestions.

Author Contributions

B.W. and H.C. conceived and designed the experiments. B.W., K.C. and B.Z. performed most of the experiments. B.W. primarily contributed to the in vivo molecular mechanism. B.W. and K.C. primarily contributed to in vitro data in atherosclerosis analysis. B.Z. prepared samples for the scRNA-sequencing and did cDNA library construction. M.D. analyzed the scRNA-seq data and performed bioinformatic work. H.W., K.L. and B.S. helped with immunostaining. Y.S. helped with the primary SMC isolation. B.W. and D.W. analyzed the data and provided comments. H.W., and Y.D. worked on part of the molecular mechanism investigation. K.L. and S.W. performed the mouse genotyping and colony maintenance. B.W., D.W., M.D., D.B.C., Y.C. and H.C. wrote and edited the article. All the authors reviewed and provided feedback on the article.

Sources of Funding

This work was supported in part by the National Institutes of Health (grants R01HL137229, R01HL1563626, R01HL158097, and R01HL146134 to Dr. Chen).

Disclosures

None.

Supplemental Material

Document S1. Figures S1–S9 and Tables S1 and S2
Table S3. Excel file containing additional data too large to fit in a PDF, related to Figure 2
Table S4. Excel file containing even more data too large to fit in a PDF, related to Figure 2
Table S5. Excel file containing even more data too large to fit in a PDF, related to Figure 2
Table S6. Excel file containing even more data too large to fit in a PDF, related to Figure 5

References

1. Frak, W., Wojtasinska, A., Lisinska, W., Mlynarska, E., Franczyk, B., and Rysz, J. (2022). Pathophysiology of Cardiovascular Diseases: New Insights into Molecular Mechanisms of Atherosclerosis, Arterial Hypertension, and Coronary Artery Disease. Biomedicines *10*. 10.3390/biomedicines10081938.
2. Kong, P., Cui, Z.Y., Huang, X.F., Zhang, D.D., Guo, R.J., and Han, M. (2022). Inflammation and atherosclerosis: signaling pathways and therapeutic intervention.

945 Signal Transduct Target Ther *7*, 131. 10.1038/s41392-022-00955-7.
946 3. Badimon, L., and Vilahur, G. (2014). Thrombosis formation on atherosclerotic lesions
947 and plaque rupture. J Intern Med *276*, 618-632. 10.1111/joim.12296.
948 4. Kowara, M., and Cudnoch-Jedrzejewska, A. (2021). Pathophysiology of
949 Atherosclerotic Plaque Development-Contemporary Experience and New Directions in
950 Research. Int J Mol Sci *22*. 10.3390/ijms22073513.
951 5. Chappell, J., Harman, J.L., Narasimhan, V.M., Yu, H., Foote, K., Simons, B.D., Bennett,
952 M.R., and Jorgensen, H.F. (2016). Extensive Proliferation of a Subset of Differentiated,
953 yet Plastic, Medial Vascular Smooth Muscle Cells Contributes to Neointimal Formation
954 in Mouse Injury and Atherosclerosis Models. Circ Res *119*, 1313-1323.
955 10.1161/CIRCRESAHA.116.309799.
956 6. Allahverdian, S., Chaabane, C., Boukais, K., Francis, G.A., and Bochaton-Piallat, M.L.
957 (2018). Smooth muscle cell fate and plasticity in atherosclerosis. Cardiovasc Res *114*,
958 540-550. 10.1093/cvr/cvy022.
959 7. Shankman, L.S., Gomez, D., Cherepanova, O.A., Salmon, M., Alencar, G.F., Haskins,
960 R.M., Swiatlowska, P., Newman, A.A., Greene, E.S., Straub, A.C., et al. (2015). KLF4-
961 dependent phenotypic modulation of smooth muscle cells has a key role in
962 atherosclerotic plaque pathogenesis. Nat Med *21*, 628-637. 10.1038/nm.3866.
963 8. Gomez, D., and Owens, G.K. (2012). Smooth muscle cell phenotypic switching in
964 atherosclerosis. Cardiovasc Res *95*, 156-164. 10.1093/cvr/cvs115.
965 9. Rong, J.X., Shapiro, M., Trogan, E., and Fisher, E.A. (2003). Transdifferentiation of
966 mouse aortic smooth muscle cells to a macrophage-like state after cholesterol loading.
967 Proc Natl Acad Sci U S A *100*, 13531-13536. 10.1073/pnas.1735526100.
968 10. Pidkovka, N.A., Cherepanova, O.A., Yoshida, T., Alexander, M.R., Deaton, R.A.,
969 Thomas, J.A., Leitinger, N., and Owens, G.K. (2007). Oxidized phospholipids induce
970 phenotypic switching of vascular smooth muscle cells in vivo and in vitro. Circ Res
971 *101*, 792-801. 10.1161/CIRCRESAHA.107.152736.
972 11. Bennett, M.R., Sinha, S., and Owens, G.K. (2016). Vascular Smooth Muscle Cells in
973 Atherosclerosis. Circ Res *118*, 692-702. 10.1161/CIRCRESAHA.115.306361.
974 12. Wirka, R.C., Wagh, D., Paik, D.T., Pjanic, M., Nguyen, T., Miller, C.L., Kundu, R.,
975 Nagao, M., Coller, J., Koyano, T.K., et al. (2019). Atheroprotective roles of smooth
976 muscle cell phenotypic modulation and the TCF21 disease gene as revealed by single-
977 cell analysis. Nat Med *25*, 1280-1289. 10.1038/s41591-019-0512-5.
978 13. Pan, H., Xue, C., Auerbach, B.J., Fan, J., Bashore, A.C., Cui, J., Yang, D.Y., Trignano,
979 S.B., Liu, W., Shi, J., et al. (2020). Single-Cell Genomics Reveals a Novel Cell State
980 During Smooth Muscle Cell Phenotypic Switching and Potential Therapeutic Targets
981 for Atherosclerosis in Mouse and Human. Circulation *142*, 2060-2075.
982 10.1161/CIRCULATIONAHA.120.048378.
983 14. Tetreault, M.P., Yang, Y., and Katz, J.P. (2013). Kruppel-like factors in cancer. Nat Rev
984 Cancer *13*, 701-713. 10.1038/nrc3582.
985 15. Alencar, G.F., Owsiany, K.M., Karnewar, S., Sukhavasi, K., Mocci, G., Nguyen, A.T.,
986 Williams, C.M., Shamsuzzaman, S., Mokry, M., Henderson, C.A., et al. (2020). Stem
987 Cell Pluripotency Genes Klf4 and Oct4 Regulate Complex SMC Phenotypic Changes
988 Critical in Late-Stage Atherosclerotic Lesion Pathogenesis. Circulation *142*, 2045-2059.

989 10.1161/CIRCULATIONAHA.120.046672.
990 16. Salmon, M., Gomez, D., Greene, E., Shankman, L., and Owens, G.K. (2012).
991 Cooperative binding of KLF4, pELK-1, and HDAC2 to a G/C repressor element in the
992 SM22alpha promoter mediates transcriptional silencing during SMC phenotypic
993 switching in vivo. Circ Res *111*, 685-696. 10.1161/CIRCRESAHA.112.269811.
994 17. Hu, D., Gur, M., Zhou, Z., Gamper, A., Hung, M.C., Fujita, N., Lan, L., Bahar, I., and
995 Wan, Y. (2015). Interplay between arginine methylation and ubiquitylation regulates
996 KLF4-mediated genome stability and carcinogenesis. Nat Commun *6*, 8419.
997 10.1038/ncomms9419.
998 18. Cherepanova, O.A., Gomez, D., Shankman, L.S., Swiatlowska, P., Williams, J.,
999 Sarmento, O.F., Alencar, G.F., Hess, D.L., Bevard, M.H., Greene, E.S., et al. (2016).
1000 Activation of the pluripotency factor OCT4 in smooth muscle cells is atheroprotective.
1001 Nat Med *22*, 657-665. 10.1038/nm.4109.
1002 19. Shin, J., Tkachenko, S., Gomez, D., Tripathi, R., Owens, G.K., and Cherepanova, O.A.
1003 (2023). Smooth muscle cells-specific loss of OCT4 accelerates neointima formation
1004 after acute vascular injury. Front Cardiovasc Med *10*, 1276945.
1005 10.3389/fcvm.2023.1276945.
1006 20. Dong, Y., Wang, B., Du, M., Zhu, B., Cui, K., Li, K., Yuan, K., Cowan, D.B.,
1007 Bhattacharjee, S., Wong, S., et al. (2023). Targeting Epsins to Inhibit Fibroblast Growth
1008 Factor Signaling While Potentiating Transforming Growth Factor-beta Signaling
1009 Constrains Endothelial-to-Mesenchymal Transition in Atherosclerosis. Circulation *147*,
1010 669-685. 10.1161/CIRCULATIONAHA.122.063075.
1011 21. Dong, Y., Lee, Y., Cui, K., He, M., Wang, B., Bhattacharjee, S., Zhu, B., Yago, T., Zhang,
1012 K., Deng, L., et al. (2020). Epsin-mediated degradation of IP3R1 fuels atherosclerosis.
1013 Nat Commun *11*, 3984. 10.1038/s41467-020-17848-4.
1014 22. Cui, K., Gao, X., Wang, B., Wu, H., Arulsamy, K., Dong, Y., Xiao, Y., Jiang, X.,
1015 Malovichko, M.V., Li, K., et al. (2023). Epsin Nanotherapy Regulates Cholesterol
1016 Transport to Fortify Atheroma Regression. Circ Res *132*, e22-e42.
1017 10.1161/CIRCRESAHA.122.321723.
1018 23. Kawai-Kowase, K., Ohshima, T., Matsui, H., Tanaka, T., Shimizu, T., Iso, T., Arai, M.,
1019 Owens, G.K., and Kurabayashi, M. (2009). PIAS1 mediates TGFbeta-induced SM
1020 alpha-actin gene expression through inhibition of KLF4 function-expression by protein
1021 sumoylation. Arterioscler Thromb Vasc Biol *29*, 99-106.
1022 10.1161/ATVBAHA.108.172700.
1023 24. Adam, P.J., Regan, C.P., Hautmann, M.B., and Owens, G.K. (2000). Positive- and
1024 negative-acting Kruppel-like transcription factors bind a transforming growth factor
1025 beta control element required for expression of the smooth muscle cell differentiation
1026 marker SM22alpha in vivo. J Biol Chem *275*, 37798-37806. 10.1074/jbc.M006323200.
1027 25. Wirth, A., Benyo, Z., Lukasova, M., Leutgeb, B., Wettschureck, N., Gorbey, S., Orsy,
1028 P., Horvath, B., Maser-Gluth, C., Greiner, E., et al. (2008). G12-G13-LARG-mediated
1029 signaling in vascular smooth muscle is required for salt-induced hypertension. Nat Med
1030 *14*, 64-68. 10.1038/nm1666.
1031 26. Deaton, R.A., Bulut, G., Serbulea, V., Salamon, A., Shankman, L.S., Nguyen, A.T., and
1032 Owens, G.K. (2023). A New Autosomal Myh11-CreER(T2) Smooth Muscle Cell

Lineage Tracing and Gene Knockout Mouse Model-Brief Report. Arterioscler Thromb Vasc Biol *43*, 203-211. 10.1161/ATVBAHA.122.318160.

27. Li, Z., Martin, M., Zhang, J., Huang, H.Y., Bai, L., Zhang, J., Kang, J., He, M., Li, J., Maurya, M.R., et al. (2017). Kruppel-Like Factor 4 Regulation of Cholesterol-25-Hydroxylase and Liver X Receptor Mitigates Atherosclerosis Susceptibility. Circulation *136*, 1315-1330. 10.1161/CIRCULATIONAHA.117.027462.
28. Stuart, T., Butler, A., Hoffman, P., Hafemeister, C., Papalexi, E., Mauck, W.M., 3rd, Hao, Y., Stoeckius, M., Smibert, P., and Satija, R. (2019). Comprehensive Integration of Single-Cell Data. Cell *177*, 1888-1902 e1821. 10.1016/j.cell.2019.05.031.
29. Korsunsky, I., Millard, N., Fan, J., Slowikowski, K., Zhang, F., Wei, K., Baglaenko, Y., Brenner, M., Loh, P.R., and Raychaudhuri, S. (2019). Fast, sensitive and accurate integration of single-cell data with Harmony. Nat Methods *16*, 1289-1296. 10.1038/s41592-019-0619-0.
30. Kaya-Okur, H.S., Wu, S.J., Codomo, C.A., Pledger, E.S., Bryson, T.D., Henikoff, J.G., Ahmad, K., and Henikoff, S. (2019). CUT&Tag for efficient epigenomic profiling of small samples and single cells. Nat Commun *10*, 1930. 10.1038/s41467-019-09982-5.
31. La Manno, G., Soldatov, R., Zeisel, A., Braun, E., Hochgerner, H., Petukhov, V., Lidschreiber, K., Kastriti, M.E., Lonnerberg, P., Furlan, A., et al. (2018). RNA velocity of single cells. Nature *560*, 494-498. 10.1038/s41586-018-0414-6.
32. Bergen, V., Lange, M., Peidli, S., Wolf, F.A., and Theis, F.J. (2020). Generalizing RNA velocity to transient cell states through dynamical modeling. Nat Biotechnol *38*, 1408-1414. 10.1038/s41587-020-0591-3.
33. Gulati, G.S., Sikandar, S.S., Wesche, D.J., Manjunath, A., Bharadwaj, A., Berger, M.J., Ilagan, F., Kuo, A.H., Hsieh, R.W., Cai, S., et al. (2020). Single-cell transcriptional diversity is a hallmark of developmental potential. Science *367*, 405-411. 10.1126/science.aax0249.
34. Qiu, X., Mao, Q., Tang, Y., Wang, L., Chawla, R., Pliner, H.A., and Trapnell, C. (2017). Reversed graph embedding resolves complex single-cell trajectories. Nat Methods *14*, 979-982. 10.1038/nmeth.4402.
35. Jin, S., Guerrero-Juarez, C.F., Zhang, L., Chang, I., Ramos, R., Kuan, C.H., Myung, P., Plikus, M.V., and Nie, Q. (2021). Inference and analysis of cell-cell communication using CellChat. Nat Commun *12*, 1088. 10.1038/s41467-021-21246-9.
36. Nelson, C.P., Goel, A., Butterworth, A.S., Kanoni, S., Webb, T.R., Marouli, E., Zeng, L., Ntalla, I., Lai, F.Y., Hopewell, J.C., et al. (2017). Association analyses based on false discovery rate implicate new loci for coronary artery disease. Nat Genet *49*, 1385-1391. 10.1038/ng.3913.
37. Nikpay, M., Goel, A., Won, H.H., Hall, L.M., Willenborg, C., Kanoni, S., Saleheen, D., Kyriakou, T., Nelson, C.P., Hopewell, J.C., et al. (2015). A comprehensive 1,000 Genomes-based genome-wide association meta-analysis of coronary artery disease. Nat Genet *47*, 1121-1130. 10.1038/ng.3396.
38. Myocardial Infarction, G., Investigators, C.A.E.C., Stitziel, N.O., Stirrups, K.E., Masca, N.G., Erdmann, J., Ferrario, P.G., Konig, I.R., Weeke, P.E., Webb, T.R., et al. (2016). Coding Variation in ANGPTL4, LPL, and SVEP1 and the Risk of Coronary Disease. N Engl J Med *374*, 1134-1144. 10.1056/NEJMoa1507652.

39. de Leeuw, C.A., Mooij, J.M., Heskes, T., and Posthuma, D. (2015). MAGMA: generalized gene-set analysis of GWAS data. PLoS Comput Biol *11*, e1004219. 10.1371/journal.pcbi.1004219.
40. Ferkingstad, E., Sulem, P., Atlason, B.A., Sveinbjornsson, G., Magnusson, M.I., Styrmisdottir, E.L., Gunnarsdottir, K., Helgason, A., Oddsson, A., Halldorsson, B.V., et al. (2021). Large-scale integration of the plasma proteome with genetics and disease. Nat Genet *53*, 1712-1721. 10.1038/s41588-021-00978-w.
41. Burgess, S., Davey Smith, G., Davies, N.M., Dudbridge, F., Gill, D., Glymour, M.M., Hartwig, F.P., Kutalik, Z., Holmes, M.V., Minelli, C., et al. (2019). Guidelines for performing Mendelian randomization investigations: update for summer 2023. Wellcome Open Res *4*, 186. 10.12688/wellcomeopenres.15555.3.
42. Hemani, G., Zheng, J., Elsworth, B., Wade, K.H., Haberland, V., Baird, D., Laurin, C., Burgess, S., Bowden, J., Langdon, R., et al. (2018). The MR-Base platform supports systematic causal inference across the human phenome. Elife *7*. 10.7554/eLife.34408.
43. Becht, E., McInnes, L., Healy, J., Dutertre, C.A., Kwok, I.W.H., Ng, L.G., Ginhoux, F., and Newell, E.W. (2018). Dimensionality reduction for visualizing single-cell data using UMAP. Nat Biotechnol. 10.1038/nbt.4314.
44. Lange, M., Bergen, V., Klein, M., Setty, M., Reuter, B., Bakhti, M., Lickert, H., Ansari, M., Schniering, J., Schiller, H.B., et al. (2022). CellRank for directed single-cell fate mapping. Nat Methods *19*, 159-170. 10.1038/s41592-021-01346-6.
45. Saelens, W., Cannoodt, R., Todorov, H., and Saeys, Y. (2019). A comparison of single-cell trajectory inference methods. Nat Biotechnol *37*, 547-554. 10.1038/s41587-019-0071-9.
46. Trapnell, C. (2015). Defining cell types and states with single-cell genomics. Genome Res *25*, 1491-1498. 10.1101/gr.190595.115.
47. Yan, D., He, Y., Dai, J., Yang, L., Wang, X., and Ruan, Q. (2017). Vascular endothelial growth factor modified macrophages transdifferentiate into endothelial-like cells and decrease foam cell formation. Biosci Rep *37*. 10.1042/BSR20170002.
48. Sayed, N., Wong, W.T., Ospino, F., Meng, S., Lee, J., Jha, A., Dexheimer, P., Aronow, B.J., and Cooke, J.P. (2015). Transdifferentiation of human fibroblasts to endothelial cells: role of innate immunity. Circulation *131*, 300-309. 10.1161/CIRCULATIONAHA.113.007394.
49. Takehara, K., LeRoy, E.C., and Grotendorst, G.R. (1987). TGF-beta inhibition of endothelial cell proliferation: alteration of EGF binding and EGF-induced growth-regulatory (competence) gene expression. Cell *49*, 415-422. 10.1016/0092-8674(87)90294-7.
50. Tobias, P.S., and Curtiss, L.K. (2007). Toll-like receptors in atherosclerosis. Biochem Soc Trans *35*, 1453-1455. 10.1042/BST0351453.
51. Khachigian, L.M. (2023). The MEK-ERK-Egr-1 axis and its regulation in cardiovascular disease. Vascul Pharmacol *153*, 107232. 10.1016/j.vph.2023.107232.
52. Pi, S., Mao, L., Chen, J., Shi, H., Liu, Y., Guo, X., Li, Y., Zhou, L., He, H., Yu, C., et al. (2021). The P2RY12 receptor promotes VSMC-derived foam cell formation by inhibiting autophagy in advanced atherosclerosis. Autophagy *17*, 980-1000. 10.1080/15548627.2020.1741202.

1121 53. Yoshida, T., Yamashita, M., Horimai, C., and Hayashi, M. (2013). Smooth muscle-
1122 selective inhibition of nuclear factor-kappaB attenuates smooth muscle phenotypic
1123 switching and neointima formation following vascular injury. J Am Heart Assoc *2*,
1124 e000230. 10.1161/JAHA.113.000230.
1125 54. Jin, Z., Li, J., Pi, J., Chu, Q., Wei, W., Du, Z., Qing, L., Zhao, X., and Wu, W. (2020).
1126 Geniposide alleviates atherosclerosis by regulating macrophage polarization via the
1127 FOS/MAPK signaling pathway. Biomed Pharmacother *125*, 110015.
1128 10.1016/j.biopha.2020.110015.
1129 55. Akoumianakis, I., Polkinghorne, M., and Antoniades, C. (2022). Non-canonical WNT
1130 signalling in cardiovascular disease: mechanisms and therapeutic implications. Nat Rev
1131 Cardiol *19*, 783-797. 10.1038/s41569-022-00718-5.
1132 56. Fu, X., Sun, Z., Long, Q., Tan, W., Ding, H., Liu, X., Wu, L., Wang, Y., and Zhang, W.
1133 (2022). Glycosides from Buyang Huanwu Decoction inhibit atherosclerotic
1134 inflammation via JAK/STAT signaling pathway. Phytomedicine *105*, 154385.
1135 10.1016/j.phymed.2022.154385.
1136 57. Srinivas, S., Watanabe, T., Lin, C.S., William, C.M., Tanabe, Y., Jessell, T.M., and
1137 Costantini, F. (2001). Cre reporter strains produced by targeted insertion of EYFP and
1138 ECFP into the ROSA26 locus. BMC Dev Biol *1*, 4. 10.1186/1471-213x-1-4.
1139 58. Hassan, H.H., Denis, M., Krimbou, L., Marcil, M., and Genest, J. (2006). Cellular
1140 cholesterol homeostasis in vascular endothelial cells. Can J Cardiol *22 Suppl B*, 35B-
1141 40B. 10.1016/s0828-282x(06)70985-0.
1142 59. Voyta, J.C., Via, D.P., Butterfield, C.E., and Zetter, B.R. (1984). Identification and
1143 isolation of endothelial cells based on their increased uptake of acetylated-low density
1144 lipoprotein. J Cell Biol *99*, 2034-2040. 10.1083/jcb.99.6.2034.
1145 60. Deaton, R.A., Gan, Q., and Owens, G.K. (2009). Sp1-dependent activation of KLF4 is
1146 required for PDGF-BB-induced phenotypic modulation of smooth muscle. Am J
1147 Physiol Heart Circ Physiol *296*, H1027-1037. 10.1152/ajpheart.01230.2008.
1148 61. Cho, D.I., Ahn, M.J., Cho, H.H., Cho, M., Jun, J.H., Kang, B.G., Lim, S.Y., Yoo, S.J.,
1149 Kim, M.R., Kim, H.S., et al. (2023). ANGPTL4 stabilizes atherosclerotic plaques and
1150 modulates the phenotypic transition of vascular smooth muscle cells through KLF4
1151 downregulation. Exp Mol Med *55*, 426-442. 10.1038/s12276-023-00937-x.
1152 62. Murgai, M., Ju, W., Eason, M., Kline, J., Beury, D.W., Kaczanowska, S., Miettinen,
1153 M.M., Kruhlak, M., Lei, H., Shern, J.F., et al. (2017). KLF4-dependent perivascular
1154 cell plasticity mediates pre-metastatic niche formation and metastasis. Nat Med *23*,
1155 1176-1190. 10.1038/nm.4400.
1156 63. Chen, Z.Y., Wang, X., Zhou, Y., Offner, G., and Tseng, C.C. (2005). Destabilization of
1157 Kruppel-like factor 4 protein in response to serum stimulation involves the ubiquitin-
1158 proteasome pathway. Cancer Res *65*, 10394-10400. 10.1158/0008-5472.CAN-05-2059.
1159 64. Gamper, A.M., Qiao, X., Kim, J., Zhang, L., DeSimone, M.C., Rathmell, W.K., and
1160 Wan, Y. (2012). Regulation of KLF4 turnover reveals an unexpected tissue-specific role
1161 of pVHL in tumorigenesis. Mol Cell *45*, 233-243. 10.1016/j.molcel.2011.11.031.
1162 65. Libby, P., and Sasiela, W. (2006). Plaque stabilization: Can we turn theory into evidence?
1163 Am J Cardiol *98*, 26P-33P. 10.1016/j.amjcard.2006.09.017.
1164 66. Brophy, M.L., Dong, Y., Tao, H., Yancey, P.G., Song, K., Zhang, K., Wen, A., Wu, H.,

1165 Lee, Y., Malovichko, M.V., et al. (2019). Myeloid-Specific Deletion of Epsins 1 and 2
1166 Reduces Atherosclerosis by Preventing LRP-1 Downregulation. Circ Res *124*, e6-e19.
1167 10.1161/CIRCRESAHA.118.313028.
1168 67. Dhaliwal, N.K., Miri, K., Davidson, S., Tamim El Jarkass, H., and Mitchell, J.A. (2018).
1169 KLF4 Nuclear Export Requires ERK Activation and Initiates Exit from Naive
1170 Pluripotency. Stem Cell Reports *10*, 1308-1323. 10.1016/j.stemcr.2018.02.007.
1171 68. Yap, C., Mieremet, A., de Vries, C.J.M., Micha, D., and de Waard, V. (2021). Six Shades
1172 of Vascular Smooth Muscle Cells Illuminated by KLF4 (Kruppel-Like Factor 4).
1173 Arterioscler Thromb Vasc Biol *41*, 2693-2707. 10.1161/ATVBAHA.121.316600.
1174 69. Salmon, M., Johnston, W.F., Woo, A., Pope, N.H., Su, G., Upchurch, G.R., Jr., Owens,
1175 G.K., and Ailawadi, G. (2013). KLF4 regulates abdominal aortic aneurysm morphology
1176 and deletion attenuates aneurysm formation. Circulation *128*, S163-174.
1177 10.1161/CIRCULATIONAHA.112.000238.
1178 70. Long, X., Bell, R.D., Gerthoffer, W.T., Zlokovic, B.V., and Miano, J.M. (2008).
1179 Myocardin is sufficient for a smooth muscle-like contractile phenotype. Arterioscler
1180 Thromb Vasc Biol *28*, 1505-1510. 10.1161/ATVBAHA.108.166066.
1181 71. Chattopadhyay, A., Kwartler, C.S., Kaw, K., Li, Y., Kaw, A., Chen, J., LeMaire, S.A.,
1182 Shen, Y.H., and Milewicz, D.M. (2021). Cholesterol-Induced Phenotypic Modulation
1183 of Smooth Muscle Cells to Macrophage/Fibroblast-like Cells Is Driven by an Unfolded
1184 Protein Response. Arterioscler Thromb Vasc Biol *41*, 302-316.
1185 10.1161/ATVBAHA.120.315164.
1186 72. Zhang, X.H., Zheng, B., Gu, C., Fu, J.R., and Wen, J.K. (2012). TGF-beta1
1187 downregulates AT1 receptor expression via PKC-delta-mediated Sp1 dissociation from
1188 KLF4 and Smad-mediated PPAR-gamma association with KLF4. Arterioscler Thromb
1189 Vasc Biol *32*, 1015-1023. 10.1161/ATVBAHA.111.244962.
1190 73. Tsai, S.Y., Clavel, C., Kim, S., Ang, Y.S., Grisanti, L., Lee, D.F., Kelley, K., and Rendl,
1191 M. (2010). Oct4 and klf4 reprogram dermal papilla cells into induced pluripotent stem
1192 cells. Stem Cells *28*, 221-228. 10.1002/stem.281.
1193 74. Kim, J.B., Zaehres, H., Wu, G., Gentile, L., Ko, K., Sebastiano, V., Arauzo-Bravo, M.J.,
1194 Ruau, D., Han, D.W., Zenke, M., and Scholer, H.R. (2008). Pluripotent stem cells
1195 induced from adult neural stem cells by reprogramming with two factors. Nature *454*,
1196 646-650. 10.1038/nature07061.
1197 75. Lee, S., Wottrich, S., and Bonavida, B. (2017). Crosstalks between Raf-kinase inhibitor
1198 protein and cancer stem cell transcription factors (Oct4, KLF4, Sox2, Nanog). Tumour
1199 Biol *39*, 1010428317692253. 10.1177/1010428317692253.
1200 76. Scholer, H.R., Ruppert, S., Suzuki, N., Chowdhury, K., and Gruss, P. (1990). New type
1201 of POU domain in germ line-specific protein Oct-4. Nature *344*, 435-439.
1202 10.1038/344435a0.
1203

Figure 1. Single-cell Transcriptomic Profiling of Aortae from *ApoE*$^{-/-}$ and *Epn1&2-SMC*^{iDKO}*/ApoE*$^{-/-}$ Mice and Cell Transdifferentiation.

(A) Mouse model construction and corresponding scRNA-seq experimental workflow. (B) Uniform Manifold Approximation and Projection (UMAP) visualization of eight major cell types of mouse aortae across varying lengths of feeding on ND or WD. Dots represent individual cells, and colors represent different cell populations. (C) Proportion of major cell types. (D) Differential gene expression *Pecam1* in various cell clusters from aortae of *ApoE*$^{-/-}$ and *Epn1&2-SMC*^{iDKO}*/ApoE*$^{-/-}$ mice. *P* value was calculated by Wilcoxon rank sum test. (E)

1213 UMAP visualization of inferred RNA velocity for eight major aortae cell clusters. (F) Fate
1214 probability of major cell types transitioning into the modSMC_EC cluster in the aortae of
1215 *ApoE*$^{-/-}$ and *Epn1&2-SMC*^{iDKO}*/ApoE*$^{-/-}$ mice inferred by *CellRank*. g, CytoTRACE scores of
1216 major cell types in aortae of *ApoE*$^{-/-}$ and *Epn1&2-SMC*^{iDKO}*/ApoE*$^{-/-}$mice with long-term WD
1217 feeding. (H) The trajectory path from SMC to modSMC_EC cells in aortae of *ApoE*$^{-/-}$ and
1218 *Epn1&2-SMC*^{iDKO}*/ApoE*$^{-/-}$ mice inferred by *Monocle2*. The trajectory direction was determined
1219 by the predicted pseudotime. The trajectories were colored by pseudotime (up) and cluster
1220 identities (down). (I-J) Cell communication networks of VEGF (I) and PECAM1 (J) signaling
1221 among major cell clusters in the aortae of *ApoE*$^{-/-}$ and *Epn1&2-SMC*^{iDKO}*/ApoE*$^{-/-}$ mice
1222 calculated using *CellChat*. WD, western diet; ND, normal diet. SMC, aortic smooth muscle
1223 cell; modSMC, modulated SMC; EC, endothelial cell.

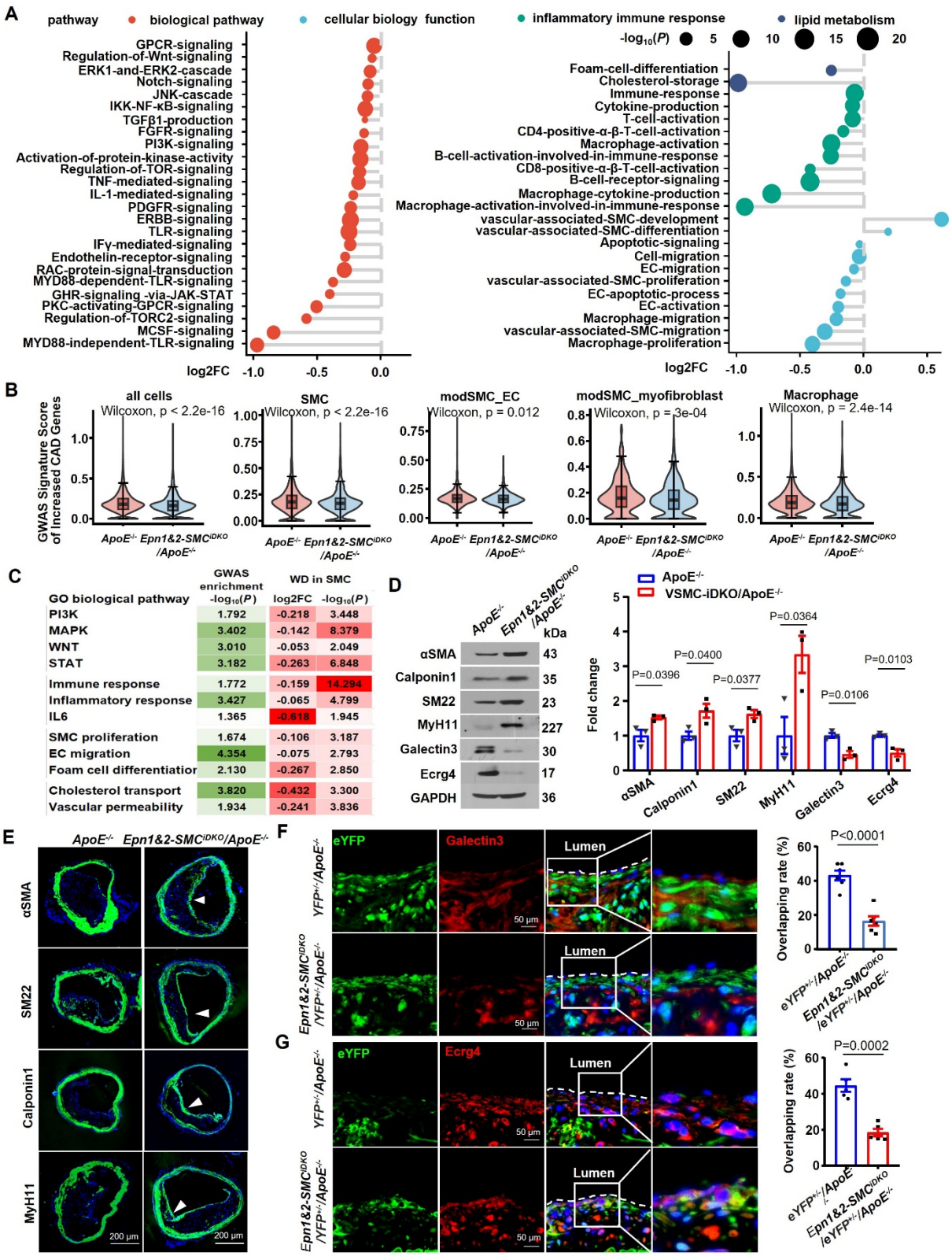

Figure 2. SMC Epsins Destabilize SMC Contraction Phenotype and Promote Atherosclerosis.

(A) GO functional annotation and pathway enrichment analysis of differentially expressed genes of scRNAseq data of aortae cells from *ApoE*$^{-/-}$ and *Epn1&2-SMC*^{iDKO}*/ApoE*$^{-/-}$mice. Each pathway was scored using *UCell* method deposited in *irGSEA* and *P* value was calculated using

Student's *t*-test. FC, fold change of pathway score by comparing *Epn1&2-SMC*^{iDKO}*/ApoE*$^{-/-}$ mice to *ApoE*$^{-/-}$ mice. (B) Combined gene expression score of the 19 CAD signature genes in the scRNAseq dataset of aortae from *ApoE*$^{-/-}$ and *Epn1&2-SMC*^{iDKO}*/ApoE*$^{-/-}$ mice across major cell types. Those 19 genes are associated with increased risk of CAD identified by GWAS of human patients as described in the text. *P* value was calculated by Wilcoxon rank sum test. (C) Enrichment scores of representative atheroprone pathways reveald by GO pathway enrichment analysis on both the 68 CAD signature genes from human GWAS and genes differentially expressed in scRNAseq data of aortae from *ApoE*$^{-/-}$ and *Epn1&2-SMC*^{iDKO}*/ApoE*$^{-/-}$mice across normal and long-term WD feeding groups. *P* value was calculated using Student's *t*-test. FC, fold change of pathway score by comparing *Epn1&2-SMC*^{iDKO}*/ApoE*$^{-/-}$ mice to *ApoE*$^{-/-}$ mice. (D) Immunoblot of VSMC markers (αSMA, Calponin1, SM22, MyH11), macrophage marker (Galectin3) and fibroblast marker (Ecrg4) in the homogenates of aortae from *ApoE*$^{-/-}$ and *Epn1&2-SMC*^{iDKO}*/ApoE*$^{-/-}$ mice fed a WD for 16 weeks. All *P* values were calculated using two-tailed unpaired Student's *t*-test. Data are mean ± s.d. n = 3 independent repeats. e, Immunofluorescence staining for α-SMA, SM22, Calponin1, and MyH11 in brachiocephalic trunk of *ApoE*$^{-/-}$ and *Epn1&2-SMC*^{iDKO}*/ApoE*$^{-/-}$ mice fed on WD for 16 weeks. Scale bar=200 μm. White arrowhead indicate SMC markers staining on fibrous cap. (F-G) Immunofluorescence staining of macrophage marker Galectin3 (F) and fibroblast marker Ecrg4 (G) in brachiocephalic trunk of YFP-tagged SMC-lineage tracing mice. Scale bar=50 μm. n=5-6 mice. SMC, aortic smooth muscle cell; EC, endothelial cell; GO, Gene Ontology; GWAS, genome-wide associated studie; CAD, coronary artery disease; WD, western diet. (D-G) All *P* values were calculated using two-tailed unpaired Student's *t*-test. Data are mean ± s.d.

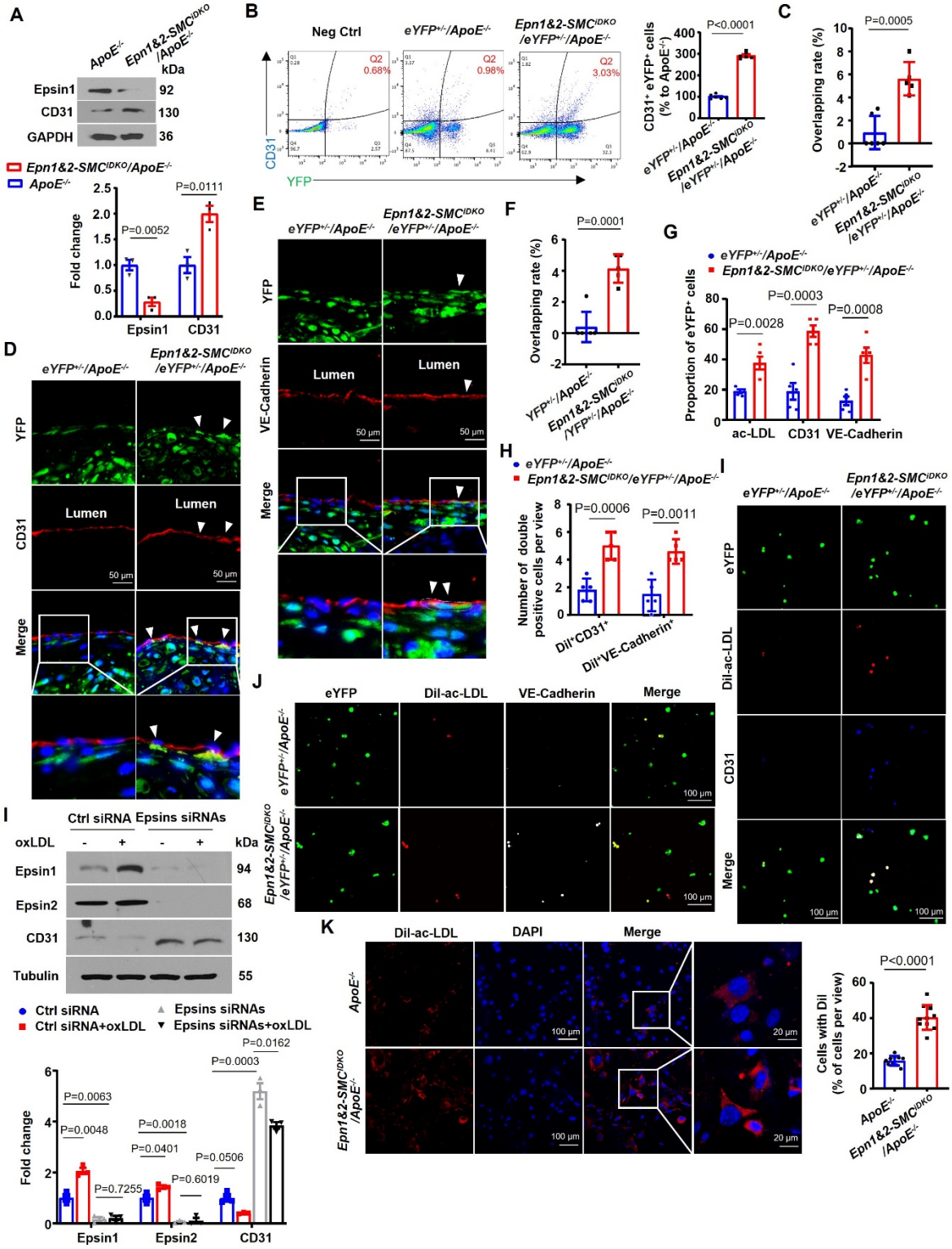

Figure 3. ModSMC_ECs Express Endothelial Markers and are Functional.

(A) Immunoblot of Epsin1 and EC marker CD31 on homogenate of aortae from *ApoE*$^{-/-}$ and *Epn1&2-SMC*^{iDKO}*/ApoE*$^{-/-}$ mice fed a WD for 16 weeks. n=3 mice. (B) Flow cytometry analysis of CD31+, YFP+ cells in aortae of *YFP*$^{+/-}$*/ApoE*$^{-/-}$ and *YFP*$^{+/-}$*/Epn1&2-SMC*^{iDKO}*/ApoE*$^{-/-}$ mice fed on WD for 14 weeks. n=6 mice. (C-F) Immunofluorescence staining of EC markers CD31 (D) and VE-Cadherin (e) on brachiocephalic trunk of *YFP*$^{+/-}$*/ApoE*$^{-/-}$ and *YFP*$^{+/-}$*/Epn1&2-*

1259 *SMC^{iDKO}/ApoE$^{-/-}$* mice fed on WD for 14 weeks. Scale bar=50 μm. n=5-6 mice. White
1260 arrowheads indicate YFP^{+} cells that are also positive for CD31 or VE-Cadherin staining. (G-J)
1261 Dil-ac-LDL uptake assays, followed by immunofluorescence staining for EC markers CD31 (I)
1262 or VE-Cadherin (J) in YFP^{+} cells sorted from total cells dissociated from aortae of *YFP$^{+/-}$/ApoE^{-}*
1263 *$^{/-}$* and *YFP$^{+/-}$/Epn1&2-SMC^{iDKO}/ApoE$^{-/-}$* mice fed on WD for 14 weeks. Scale bar=100 μm. (G)
1264 Quantification of the proportion of dil^{+}, CD31^{+} or VE-Cadherin^{+} cells in YFP^{+} cells as well as
1265 (H) the number per view of dil, YFP, CD31 or VE-Cadherin triple positive cells. n=5 mice. (K)
1266 Immunoblot of total cell lysate of primary SMC transfected with control or small interference
1267 RNAs against Epsin1&2 followed by 100 μg/mL oxLDL stimulation with antibodies indicated.
1268 Quantification values were normalized to tubulin expression levels. n=3 independent repeats.
1269 (L) Dil-ac-LDL uptake in *in vitro* cultured primary VSMCs from the aortae of *ApoE$^{-/-}$* and
1270 *Epn1&2-SMC^{iDKO}/ApoE$^{-/-}$* mice. Scale bar=100 and 20 μm, respectively. n=10 independent
1271 repeats. SMC, aortic smooth muscle cell; EC, endothelial cell; WD, western diet; Dil-ac-LDL,
1272 Dil-acetylated-low density lipoprotein; oxLDL, oxidized low-density lipoprotein. All *P* values
1273 were calculated using two-tailed unpaired Student's *t*-test. Data are mean ± s.d.

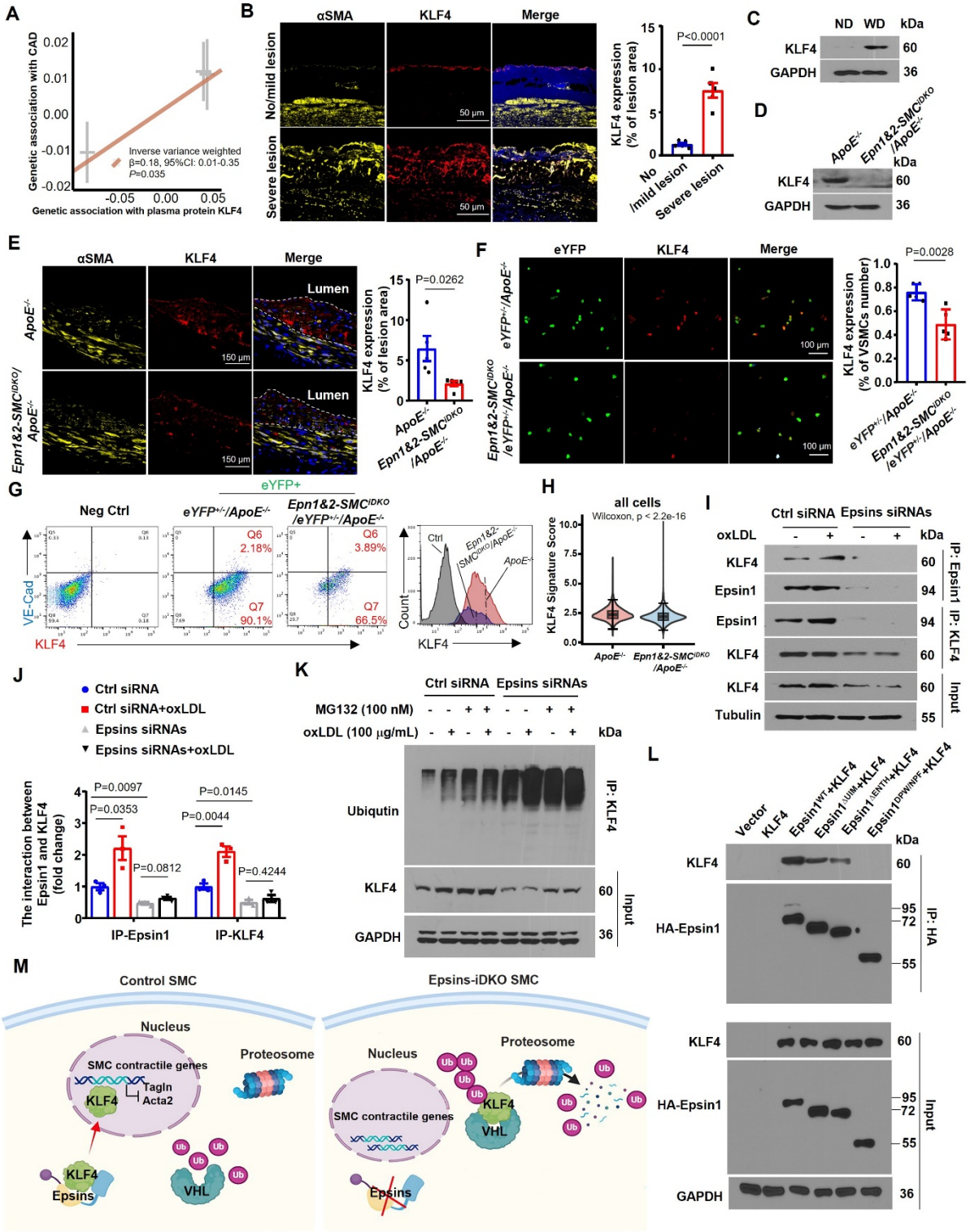

Figure 4. Epsins Stabilizes KLF4 by Interfereing with KLF4 Ubiquitination.

(A) Scatter plots for Mendelian Randomization analysis illustrating a putative causal association between plasma KLF4 protein and CAD risk. *P* value was calculated with inverse variance weighted regression using *TwoSampleMR*. (B) Immunofluorescence staining of KLF4 and α-SMA in aortae from patients with no/mild or severe atherosclerotic lesions. Scale bar=50 μm. n=5 samples. (C-D) Immunoblot of KLF4 in the homogenates of aortae from *ApoE*$^{-/-}$ mice fed on ND or WD (C) and *ApoE*$^{-/-}$ and *Epn1&2-SMC*^{iDKO}*/ApoE*$^{-/-}$ mice fed on WD for 16 weeks

(D). (E) Immunofluorescence staining for KLF4 in brachiocephalic truncks of SMC-lineage tracing *YFP*$^{+/-}$/*ApoE*$^{-/-}$ and *Epn1&2-SMC*^{iDKO}/*YFP*$^{+/-}$/*ApoE*$^{-/-}$ mice fed on WD for 14 weeks. Scale bar=150 μm. n=5 mice. (F) Immunofluorescence staining of KLF4 in sorted YFP-tagged cells from the aortae of *YFP*$^{+/-}$/*ApoE*$^{-/-}$ and *Epn1&2-SMC*^{iDKO}/*YFP*$^{+/-}$/*ApoE*$^{-/-}$ mice fed on WD for 14 weeks. Scale bar=100 μm. n=5 mice. (G) Flow cytometry plots of VE-Cadherin^{+} and KLF4^{+} cells in cells gated for YFP-postive in total cells dissociated from aortae of *YFP*$^{+/-}$/*ApoE*$^{-/-}$ and *Epn1&2-SMC*^{iDKO}/*YFP*$^{+/-}$/*ApoE*$^{-/-}$ mice fed on WD for 14 weeks. n=6 mice. (H) Differential signature score of KLF4 binding genes between *ApoE*$^{-/-}$ and *Epn1&2-SMC*^{iDKO}/*ApoE*$^{-/-}$ mice, as revealed by scRNA-seq data. *P* value was calculated by Wilcoxon rank sum test. The signature score was calculated on 1113 target genes with KLF4 binding sites in regulatory regions with *PercentageFeatureSet* function deposited in *Seurat*. (I-J) The interaction between Epsin and KLF4 in primary SMCs from *ApoE*$^{-/-}$ and *Epn1&2-SMC*^{iDKO}/*ApoE*$^{-/-}$ mice treated with 100 μg/mL oxLDL evaluated with immunoprecipitation followed by western blot. n=3 independent repeats. (K) The KLF4 ubiquitination levels in wild type SMCs transfected with control siRNA or Epsin 1&2 siRNAs following treatment with 100 nM MG132 or 100 μg/mL oxLDL were measured by immunoprecipitation and western blot. (L) HA-tagged Epsin 1 or Epsin 1 domains were co-transfected with pCX4-KLF4 into HEK 293T cells, after 24 hrs, cell lysis was immunoprecipitated with HA antibody, followed by western blot with KLF4 and HA antibodies. (M) Schematic diagram of the proposed mechanism. Epsins stabilize KLF4 and hinder KLF4 ubiquitination by binding to KLF4 through UIM and ENTH domains of Epsin. SMC, aortic smooth muscle cell; EC, endothelial cell; WD, western diet; ND, normal diet; CAD, coronary artery disease; siRNA, small interfering RNA; oxLDL, oxidized low-density lipoprotein. All *P* values were calculated using two-tailed unpaired Student's *t*-test except (H). Data are mean ± s.d.

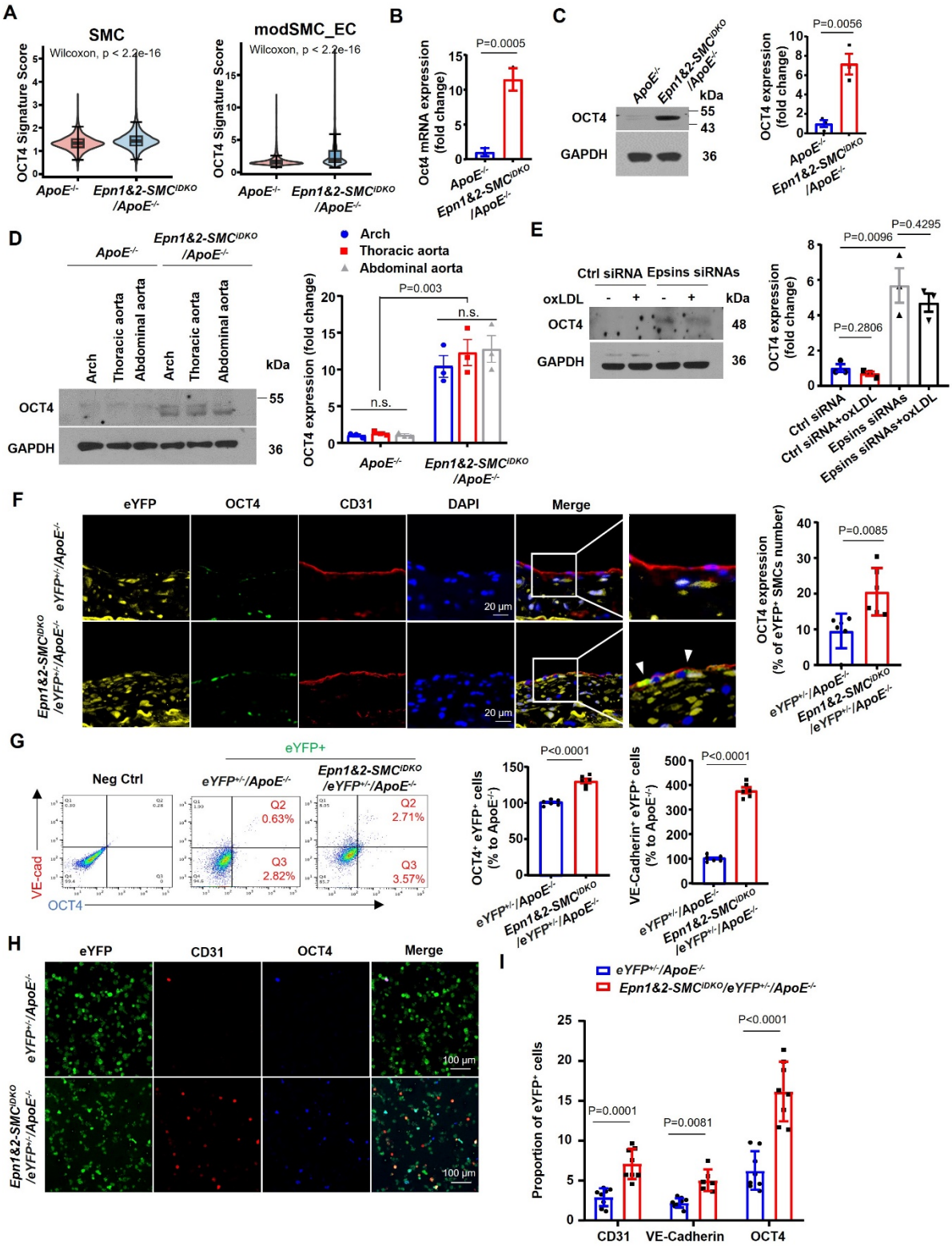

Figure 5. SMC-specific Epsins Deficiencies Promotes Expression of EC Markers in SMCs by Augmenting the OCT4 Expression in Atherosclerotic Plaques.

(A) Differential signature score of OCT4 binding genes between *ApoE*$^{-/-}$ and *Epn1&2-SMC*^{iDKO}*/ApoE*$^{-/-}$ mice across cell types of SMC and modSMC_EC derived from scRNA-seq data. *P* value was calculated by Wilcoxon rank sum test. The signature score was calculated

using 898 target genes with OCT4 binding sites in regulatory regions with *PercentageFeatureSet* function deposited in *Seurat*. (B) Relative mRNA level of Oct4 in the cells isolated from the aortae of *ApoE*$^{-/-}$ and *Epn1&2-SMC*^{iDKO}*/ApoE*$^{-/-}$ mice fed a WD for 16 weeks. n=3 mice with independent repeats. (C-D) Immunoblot analysis of OCT4 expression in either the homogenates of whole aortae (C) or different parts of aortae (D) of *ApoE*$^{-/-}$ and *Epn1&2-SMC*^{iDKO}*/ApoE*$^{-/-}$mice fed a WD for 16 weeks. n=3 mice with independent repeats. E, Immunoblot analysis of OCT4 in primary SMC isolated from the aortae of *ApoE*$^{-/-}$ and *Epn1&2-SMC*^{iDKO}*/ApoE*$^{-/-}$ mice stimulated with or without 100 μg/mL oxLDL for 24 hrs. (B-E) n=3 mice. (F) Immunofluorescence staining of OCT4 in brachiocephalic trunks of YFG-tagged SMC-lineage tracing mice with 14-week WD. Scale bar=20 μm. g, Flow cytometry plots of VE-Cadherin^{+} and Oct4^{+} in YFP^{+} cells in total cells dissociated from aortae of *YFP*$^{+/-}$*/ApoE*$^{-/-}$ and *Epn1&2-SMC*^{iDKO}*/YFP*$^{+/-}$*/ApoE*$^{-/-}$ mice fed on WD for 14 weeks. (H) Localization of Oct4 and CD31 in sorted YFP^{+} cells from total cells dissociated from aortae of *YFP*$^{+/-}$*/ApoE*$^{-/-}$ and *Epn1&2-SMC*^{iDKO}*/YFP*$^{+/-}$*/ApoE*$^{-/-}$ mice fed on WD for 14 weeks. Scale bar=100 μm. (I) Quantitation of the proportion of CD31^{+}, VE-Cadherin^{+} and OCT4^{+} in YFP^{+} cells. n=6-8 mice. (F-H) n=6 mice. SMC, aortic smooth muscle cell; EC, endothelial cell; WD, western diet; oxLDL, oxidized low-density lipoprotein. All *P* values were calculated using two-tailed unpaired Student's *t*-test except (A). Data are mean ± s.d.

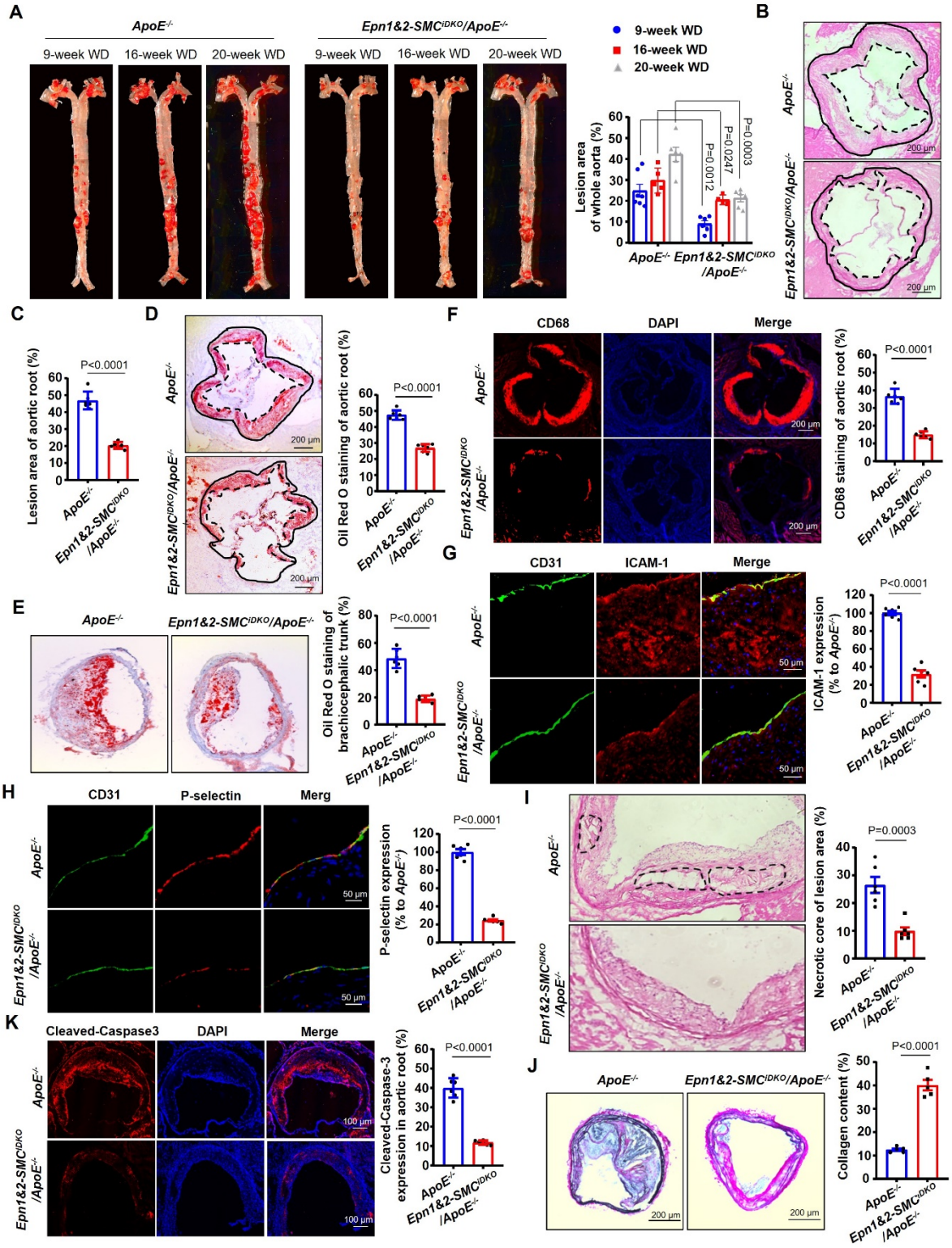

Figure 6. SMC-specific Epsin1&2 Deficiency Reduces Atherosclerotic Plaques and Enhances the Stability of Lesions in Mice.

ApoE$^{-/-}$ and *Epn1&2-SMC*^{iDKO}*/ApoE*$^{-/-}$ mice were fed a WD for 9, 16 and 20 weeks. The sections of aortic root and brachiocephalic trunks were collected from the *ApoE*$^{-/-}$ and *Epn1&2-SMC*^{iDKO}*/ApoE*$^{-/-}$ mice fed a WD for 16 weeks. (A) *En face* Oil Red O staining of the whole aortae was calculated. (A)The sections of aortic root and brachiocephalic trunks were collected

stained en face with Oil Red O. (B-C) Hematoxylin and eosin staining of aortic roots showed the size of atherosclerotic lesion. (D-E) Oil Red O staining of aortic roots (D) and brachiocephalic trunks (E) were used to show the lipid accumulation in the lesionof aortae of *ApoE*$^{-/-}$ and *Epn1&2-SMC*^{iDKO}*/ApoE*$^{-/-}$ mice fed on WD for 16 weeks. (F) Immunofluorescence staining of CD68 were performed to show the inflammation in the lesion of aortic root from aortae of *ApoE*$^{-/-}$ and *Epn1&2-SMC*^{iDKO}*/ApoE*$^{-/-}$ mice fed on WD for 16 weeks. (G-H) Immunofluorescence staining for CD31 and ICAM-1 (G) or P-selectin (H) in dissected aortic roots from aortae of *ApoE*$^{-/-}$ and *Epn1&2-SMC*^{iDKO}*/ApoE*$^{-/-}$ mice fed on WD for 16 weeks. Scale bar=50 μm. (I) Hematoxylin and eosin staining of aortic roots showed the necrotic cores in the lesion. Necrotic cores were outlined in black dash. (J) Verhoeff-Van Gieson's staining of brachiocephalic trunks was performed to show the stability of the lesion of aortae from *ApoE*$^{-/-}$ and *Epn1&2-SMC*^{iDKO}*/ApoE*$^{-/-}$ mice fed on WD for 16 weeks. Scale bar=200 mm. (K) Immunofluorescence staining of cleaved (active)-caspase3 in aortic root from *ApoE*$^{-/-}$ and *Epn1&2-SMC*^{iDKO}*/ApoE*$^{-/-}$ mice fed on WD for 16 weeks. Scale bar=100 μm. SMC, aortic smooth muscle cell; EC, endothelial cell; WD, western diet. All *P* values were calculated using two-tailed unpaired Student's *t*-test. Data are mean ± s.d. n=6 mice.

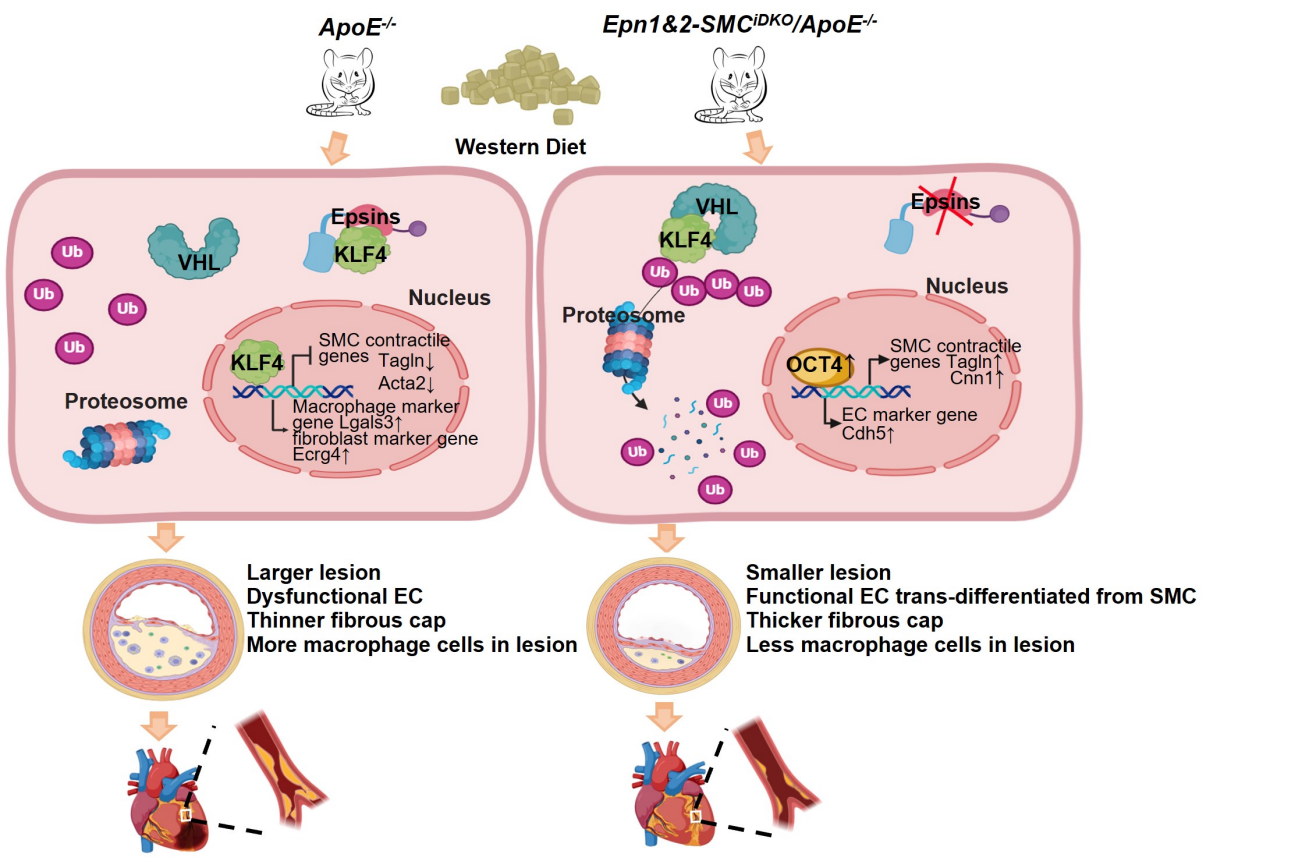
ApoE-/-
Epn1&2-SMCiDKO/ApoE-/-
Western Diet
Ub
VHL
Epsins
KLF4
Nucleus
Proteosome
SMC contractile genes
Tagln↓
Acta2↓
Macrophage marker gene Lgals3↑
fibroblast marker gene Ecrg4↑
OCT4↑
SMC contractile genes Tagln↑
Cnn1↑
EC marker gene Cdh5↑
Larger lesion
Dysfunctional EC
Thinner fibrous cap
More macrophage cells in lesion
Smaller lesion
Functional EC trans-differentiated from SMC
Thicker fibrous cap
Less macrophage cells in lesion